# NUMERICAL AND EXPERIMENTAL STUDY OF WAVE SHAPER EFFECTS ON DETONATION WAVE FRONT


**By**

**Khalid Naeem**

**School of Chemical and Materials Engineering (SCME)**

**National University of Sciences and Technology (NUST)**

**2016**

# NUMERICAL AND EXPERIMENTAL STUDY OF WAVE SHAPER EFFECTS ON DETONATION WAVE FRONT


| Name | Reg. No. |
|---|---|
| Khalid Naeem | NUST201363030MSCME67613F |


**This work is submitted as a MS thesis in partial fulfilment of the requirement for the degree of**

**(MS in Energetic Materials)**

**Supervisor Name: Engr. Dr. Arshad Hussain**


**School of Chemical and Materials Engineering (SCME)**

**National University of Sciences and Technology (NUST), H-12**

**Islamabad, Pakistan**


**January, 2016**

# Thesis Submission Certificate

It is to certify that work in this thesis has been carried out by **Mr. Khalid Naeem** and completed under my supervision in school of chemical and materials engineering, National University of Sciences and Technology, H-12, Islamabad, Pakistan.

Supervisor:_____

**Engr. Dr. Arshad Hussain**

**H.O.D Chemical Engineering**

**Submitted Through**

**Principal/Dean**

Materials Engineering Department

National University of Sciences and Technology

# Acknowledgements

All praises for The Almighty Allah who is the source of all knowledge and wisdom Who endowed some knowledge to mankind as a whole and to the Holy Prophet Muhammad ﷺ.

I will take this opportunity to express thanks to my respected teachers, friends, colleagues my family members who helped and guided me either in performing experiment or in the preparation of this thesis. I am thankful to my GEC members especially to my supervisor Dr. Arshad Hussain and co supervisor Dr. Shakeel Abbas for their continuous guidance.

Khalid Naeem.

# TABLE OF CONTENTS

# List of Figures

# List of Tables

# ABSTRACT

Objective of the current study is to observe detonation wave front by streak camera at the interface of liner and explosive during the course of high explosive detonation in two experiments one without wave shaper and other with wave shaper. Streaks were studied for concentricity between the casing, high explosive and the liner. Although the liner is replaced with the perspex mask, results will clearly reflect the concentricity of explosive and liner. Streaks were also studied for the porosity and cracks in the high explosive. To observe these effects circular grooves were machined on the perspex mask at predefined locations.

Grooves machined on the perspex mask were circular but the recorded streaks were elliptical in shapes. This happened because of the viewing angle of the camera. It was observed from the width of the streaks along the periphery of the circles that there was no porosity in the high explosive. Circular streaks also revealed that the assembly was perfectly coaxial along the whole length of the casing during the detonation of high explosive. On the basis of streaks obtained by rotating mirror camera (RMC) shock front arrival velocities were calculated; deviation between the shock front arrival velocities taken at specified location on the surface of the liner in experiment without wave shaper is ± 0.554. Same data taken from the simulation gave a standard deviation of ± 0.464. Similarly the standard deviation between the shock front arrival velocities taken at specified location on the surface of the liner in experiment with wave shaper is ±0.489 and when the data from simulation was analysed it gave a deviation of ±0.367. Standard deviation among velocities obtained from experiment with wave shaper has less variation as compared to experiment without wave shaper both in experiment and simulation.

It was observed that the shock front velocity increased by 20.87 % when wave shaper was incorporated. Increased shock front velocity is an indication of the top attack. This velocity increase is much higher near the apex of the cone, which is in agreement with the simulation. Apex is the region which contributes to the jet formation; as a result of this top attack the jet length vis a vis penetration increases which can be verified by penetration experiments.

# Introduction

Advancements in shaped charges are required to defeat newly developed reactive, homogeneous and heterogeneous armour. This can be fulfilled by improving the penetration capability of shape charges and kinetic energy penetrator. Many techniques are available to diagnose and improve the designs and manufacturing techniques. In present study the manufacturing is carried out using available lathe and milling machines. Streak cameras will be used to diagnose the effect of wave shaper on the detonation wave front, these effects will affect the properties of jet thus produced.

## 1.1 Shaped Charges and EFPs

Shaped charges mainly consists of a conical or linear metal liner, conforming high explosive and casing. With the help of energy released from the explosive; metallic liner is converted to a hypervelocity jet having velocity of Mach six or even more which penetrate the armour plate. Its penetration mainly depends on the geometry of high explosive [1].

Explosively formed penetrator (EFP) is also a type of shaped charge intended to penetrate armour effectively at certain standoff distance. Function of the explosive

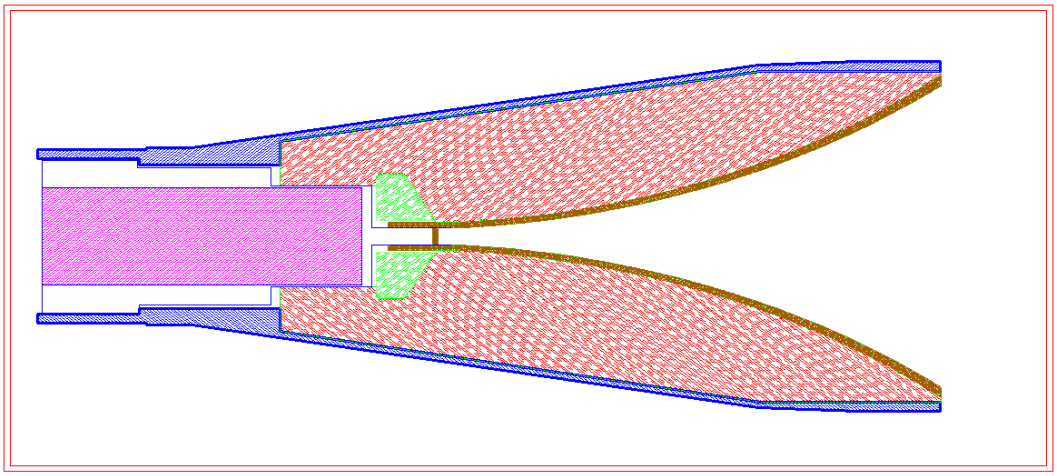

charge used in EFP is to deform a metal liner into a slug which is accelerated toward the target.[2]

Figure 1-1 Cross section view of shaped charge

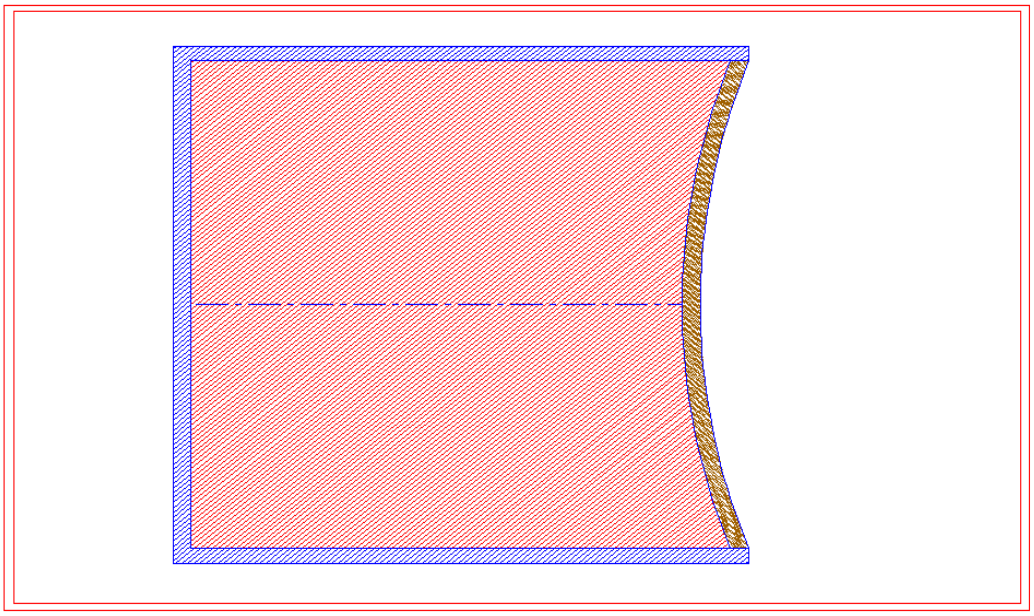

Figure 1-2 Cross section view of a typical EFP

With the help of wave shaping the liner can be moulded into any desired shape. The final shape of EFP also depends upon the initial shape of liner and explosive, thickness of the casing and the type of material used for liner, casing and explosive. As a rule of thumb, an EFP will penetrate a thickness of armour steel equal to half of its charge diameter for a copper or iron liner while it is equal to one diameter of its charge for a tantalum liner, whereas shaped charge will penetrate through six or more charge diameters.

The penetration power of shaped charges is proportional to the length of the jet formed and to the square root of the density of the liner material [3]. Therefore material like tantalum having density of 16.654 g/cm3 will give more penetration than copper and iron having densities of 8.960 g/cm3 and 7.874 g/cm3 respectively. Moreover the small conical shaped charges are mostly optimized by the introduction of wave shaper which is the area of interest and it will be while large diameter shaped charges are optimized by varying the liner geometry and liner thickness [4]. Optimization of jet can be performed by reducing the slug; in this technique cone is made of two metals; the surface which contacts the explosive disintegrate after sometime while the inner material which is away from the high

explosive contributes to the penetration in the target [5]. In order to get maximum penetration from shaped charges, the jet so produced must be extremely straight and there should be no transvers perturbations so that the jet should not hit the crater wall [6].

## 1.2 Shaped Charges Jet Formation

After the explosive has been detonated, the detonation wave propagate in the explosive and finally transferred to the liner as a result liner is accelerated with a small angle to the liner-charge interface [7]. This process is schematically presented in Figure 1-3.

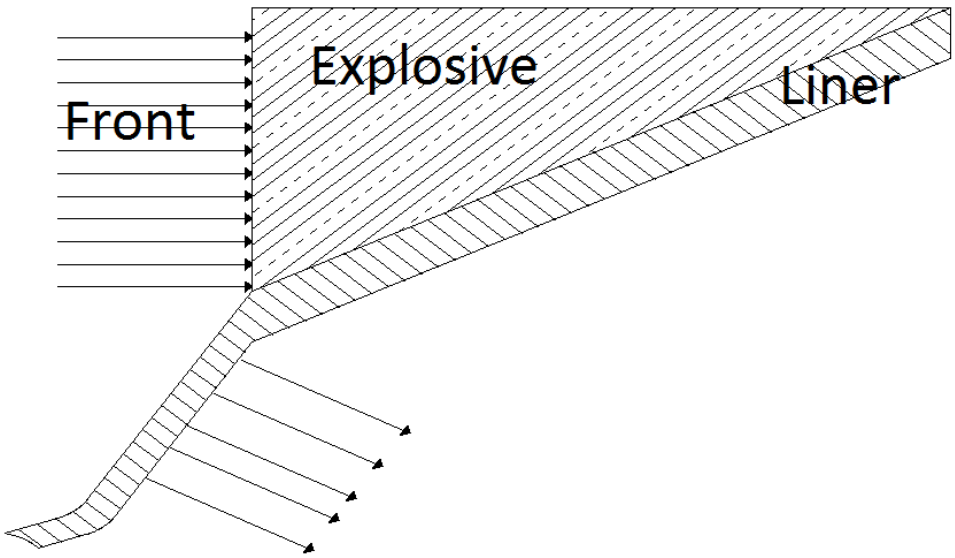


Figure 1-3 Liner Acceleration with Detonation Front

This process continues till the entire explosive is consumed and the liner is converted into a hypervelocity jet, the jet is then used for various purposes like armour penetration, oil well perforation, demolition of buildings and bridges and avalanche stimulus. Jet formation process can be best understood with the help of following chronological shaped charge formation process. These snaps have been taken from the simulation of shaped charge. A simulation for the shaped charge was run on Ansys Autodyn Euler Solver. In most of the numerical simulation jet formation, fragmentation, and the penetration is best observed by the Lagrangian solver [8]. But Lagrangian solver has the drawback of mesh tangling, so to avoid this tangling effect; Euler solver was used. Material used for liner, wave shaper,

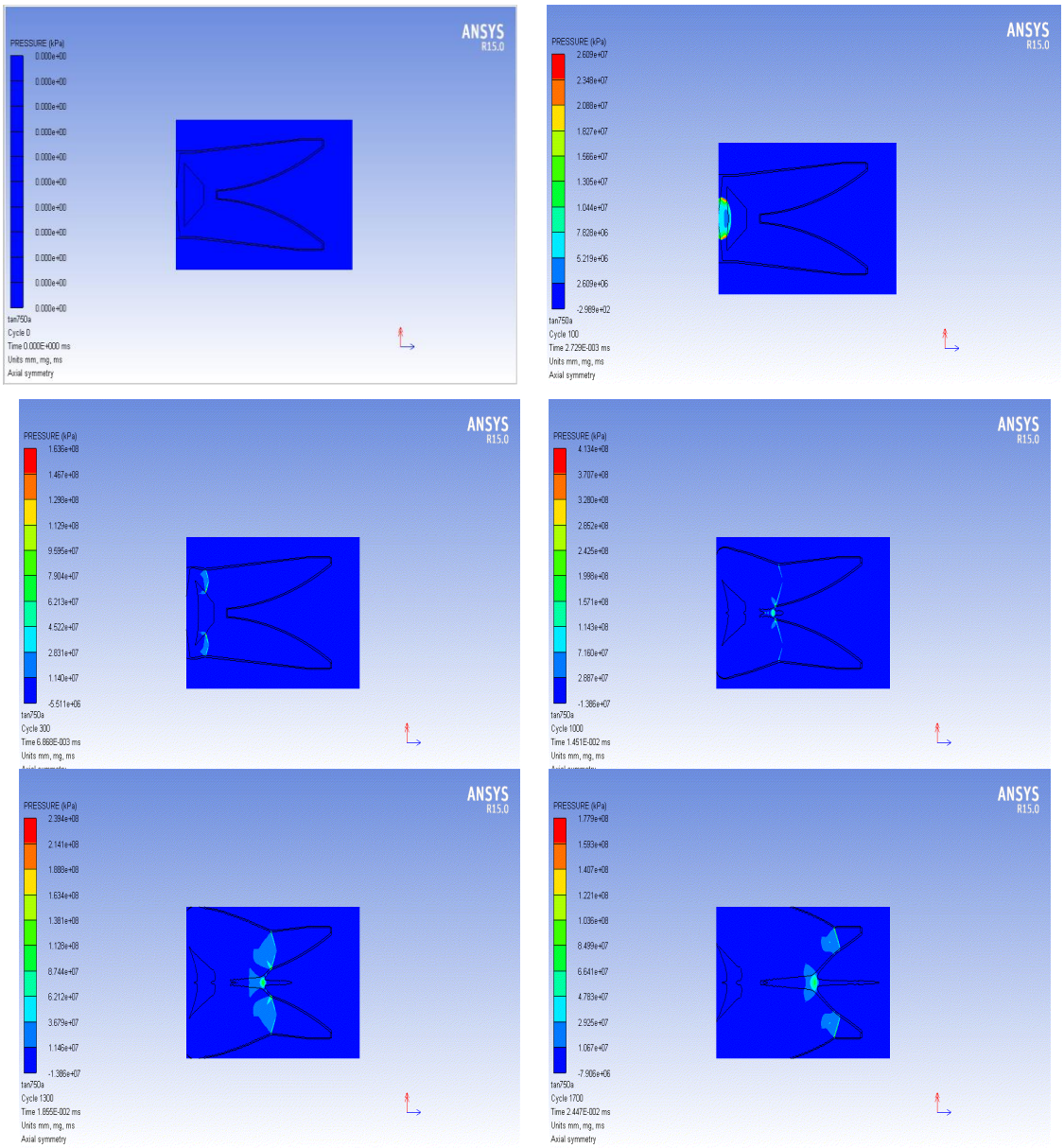


Figure 1-4 Chronological shaped charge formation process

casing and explosive materials for simulation were taken from the Ansys Autodyn library as copper (CU OFHC), aluminium (Al-2024) perspex (Plexiglass) and HMX respectively. Shock equation of state for the liner casing and wave shaper was used while Lee and Tarver equation of state was used for HMX. Jet formation and wave shaping both can be observed from pressure plots given in Figure 1-4. It also shows that wave is turning around the wave shaper and finally hit the liner from top. With the passage of time jet is formed and its length increases.

## 1.3 Applications of Shaped Charges

### 1.3.1 Military Application

Shaped charges are used in variety of High Explosive Anti-Tank (HEAT) projectiles such as 106-RR, Tandem and Rocket Propelled Grenade. It is also deployed in Smart Munition/Bomb having multiple shaped charges. Purpose of the shaped charge is to penetrate the body or armoured wall of the target. In case of HEAT attack, jet is the main damaging factor to the inside personnel and components [9]. Working principle of smart bomb is that it first identifies the target and then engages it with multiple/single shaped charge/s accordingly. Smart bombs are normally used against area targets such as runways, jet fighters on the ground and enemy formations. Shaped charges are also used underwater in the shape of torpedo. Shaped charges are also used against underground bunkers, in this case the front end of the missile or carrier is kinetic energy penetrator and the back end consists of shaped charge.

### 1.3.2 Civil Applications

Shaped charges are used for demolition purpose to carry out precision demolition for caving in of old buildings. These are also used to demolish bridges, railway track and towers for civil and military uses. Shaped charges used for cutting purposes are called linear shaped charges which are either wedge, V or W shaped. Charge without liner (hollow charge) is used in mud-capping (breaking rocks). These are used in oil rigs to increase and ease the flow of crude oil to rig. These are used in hypervelocity impact studies. Since there is no other means to accelerate a mass of even one gram or more to a velocity of 10 km/s or more [10]. Shaped charges are also used in tapping steel furnaces. Another useful application of the shaped charges is to use it as an avalanche stimulus for the safeguard of humans.

# Research Methodology

## 2.1 Introduction

A brief timeline of shape charge development is discussed. Huge amount of literature is available on the early shaped charge work which is still relevant. These references are provided which would act as starting points for further research.

## 2.2 History of Shaped Charges

The cavity effect in explosives has been the subject of regular investigations for well over 150 years and has been discovered by many people during that time. The earliest available work is that of a mining engineer from Norway who towards the end of the 18th century presented a design leaving a conical or mushroom-shaped air space under the forward end of a main charge. This conical or mushroom space increased the explosive effect and at the same time reduced considerable amount of explosive [11]. Hausmann took the idea from Norway to Germany in the early 19th century, but it was not fruitful in the Harz mines. In 1874 Davey and Watson took out a British Patent (No.2641) in which they claimed it a new invention, "The use of a cylindrical charge with a central hole below and in the middle". In 1883 Max von Foerster discovered a similar effect, known as Munroe in Washington. Munroe's work, first mentioned in an article published in 1885 showed that any pattern in the base of explosive charge was reproduced as an indentation in the underlying metal plate when the charge was detonated as shown in Figure 2-1.

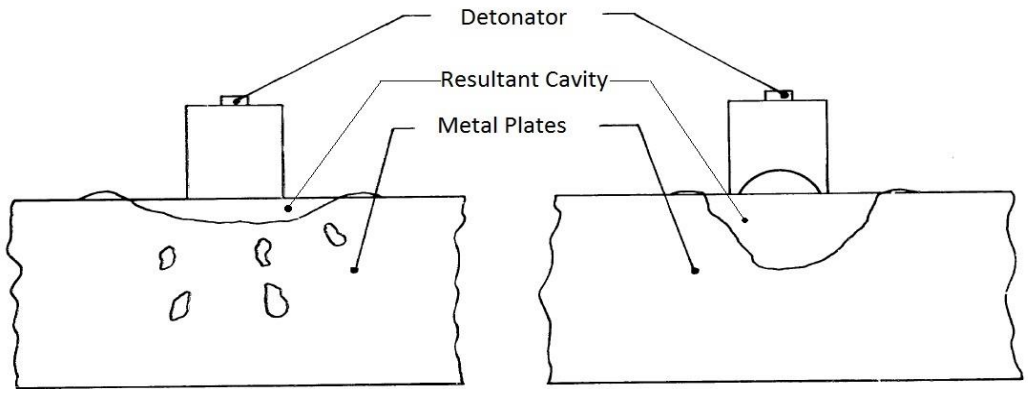


Figure 2-1 Effect of Solid and Hollow Charges on metal plate [12]

He performed his experiments on the effect of different sized holes in wet guncotton cylinders and noticed that when holes in the guncotton were deeper and wider the bored hole in the iron plate was also deepened. When the hole was through in the guncotton cylinder the iron plate was completely perforated. In 1911 M. Neumann mentioned the discovery that a hole in explosive body towards the object to be attacked increased the penetration effect three to four times. Another scientist E. Neumann published the effect of hollowing out explosive charges in 1914, which he claimed to be an entirely new method developed by his company. Although it was already discussed by German Patent No. 249,630 in 1910 and a British Patent No 28,030 .in December 1911. It could not be concluded that either Munroe or Neumann discovered the lined cavity effect. British Navy studied shaped charges in 1913 for a torpedo warhead but the technology did not advanced significantly although the claims made were confirmed. The British Army considered that the use of hollow charges in projectiles was impractical because it would be difficult to prevent the forward set of the charge on impact. At that time it was convention to place the fuse at the nose which was not possible in such cases. The enhanced effect was stated due to a more complete detonation of the explosive and it was considered that such effect could be obtained by using a more powerful detonator. Research in the field of shaped charges then declined. Then in late 1930s serious efforts were made to exploit lined shaped charges for military applications. Payman and Woodhead in 1937 working with unlined charges showed the importance of solid particles carried in the detonation products in producing and prolonging the intense end effects. They observed with the help of spark photography that the mean axial speed of the wave sent out into the atmosphere from a fully wrapped cartridge was 2010 m/s, while that from a cartridge with a conical indentation was 2740 m/s. It was also found that the end effects were even more significant when the hollow charge was lined with material. In 1938 Dr Mohaupt, claimed to the British that he had discovered a new and powerful explosive. In January 1939 two scientists from Woolwich Arsenal witnessed a demonstration by Dr Mohaupt. The projectiles exploded on contact with the plate leaving a small hole right through the armour. To conceal his achievement he added dye to the explosive to mislead the scientists who were observing the experiment. The Woolwich scientists concluded that what they had

seen was due to a hollow charge effect and not because of a new explosive. British were able to produce results similar to Dr. Mohaupt in static trials. It is however not clear that whether Dr. Mohaupt was using a lined cavity or whether the British start using lined cavities at Woolwich. In 1939 Dr. Mohaupt and Mr.Kauders applied for a French Patent for an "improved explosive projectile" which was similar in design to that submitted to the British Government. Mohaupt carried on his research in early developments of the lined cavity effect in America during the start period of World War II.

## 2.3 Use of Shaped Charges In Weapons

After the demonstration of Mohaupt the British reconsidered to introduce shaped charges into weapons used in the armed forces, particularly using plastic explosive which was very attractive for demolitions and other applications because of its easy mouldability in any shape. During static trials the Grenades penetrated 52mm of armour but when fired dynamically penetration reduced to 44mm. It was equal to 1.6 and 1.3 charge diameters. The Weapon has a range of only 300 feet. Yet having these limitations it was considered a useful weapon against armour. It was commissioned to British Defence in November 1940 as the No 68 grenade which was the world's first anti-tank hollow charge, rifle grenade. With the passage of time armours thicker than 44mm were introduced which made this British anti-tank rifles useless for their intended task. In 1941 two prototype anti-tank devices appeared, both almost same in appearance and principle. One was designed by Watts, the other by Jeffries. It consists of thin tubular steel housing the firing spring and trigger mechanism. At the front was a trough to hold the bomb and the spigot projected down the middle of the trough. The bombs had a hollow tail boom with a small cartridge at the front end. The hollow charge warhead was larger in the Jeffries version. The tube recock itself at the cost of backward jerk so another bomb could be slipped into the tube and shooting can be continued. The gun produced for production version was a .blend of Watts and Jeffries designs. It has fewer advantages over the previous version .i.e. a little muzzle flash and no back blast. It was safe to fire in confined spaces. It was named as Projector Infantry Anti-Tank or PIAT. It had short range but the shaped charge bomb could penetrate

any tank armour existing at that time. This was a noteworthy achievement of British in 1940.

## 2.4 Period Of World War II

By noticing the damage produced by jets in heavy steel targets at different standoff Evans and Ubbelohde deduced the mechanism of Jet structure and jet formation [12]. With the help of photograph they found that when hollow charges without liner were detonated, a thin pencil-like flame was projected along the axis of the charge. Velocity of the pencil like flame near the charge was high but it reduced rapidly in the air. Due to this reason in early experiments charge was kept in contact with the target. When the high explosive was loaded with a metal liner, the crater in the target increased intensely. Depth of the crater was also increased when lined explosive was moved away from the target. This put forward the idea that when explosive was detonated liner formed some kind of projectile which continued in space after the explosive products had dissipated. This phenomenon was not clear to the researchers so to make it clear vaporisation of projectiles were studied by firing liners with increasing boiling points. From these experiments it was concluded that the determinant factor in penetration was the ductility of liner, not it's boiling point and the process of collapse of the liner appeared to be complete within a distance of one to two charge diameters, depending on the shape, thickness and metal used as liner. Later on these assumptions were confirmed with flash radiography. Projectiles were recovered after travelling some distance in air which gave enough information about various aspects of jet formation and jet structure. The recovered jets from conical liners consisted of a plug of metal, which accounted for a considerable amount of mass. In 1943 Kolsky, Shearman and Snow in England concluded while studying jet formation that the liner accelerates rapidly towards its base. The metallic liner was crushed in such a way that it turned back and formed a sharp jet. Turning back of the cone walls was confirmed by using bimetal liners. It was observed that jet formed by the bimetallic liner initially having steel at the inner side of cone and copper on the exterior of cone has characteristics of the steel while the slug has steel on the inner side and copper on the outer. Kolsky in 1944 wrote a paper on the collapse of hemispherical liners

## 2.5 Post War Period

As jet gets its entire energy from the chemical energy of the main charge so Evans and Ubbelohde gave a hypothesis that more powerful explosives would improve the penetration of the jet. It was confirmed by using different types of explosives in the shaped charges. They also observed that a firm contact between liner and explosive gives better results in terms of jet formation and penetration while poor contact resulted in asymmetric jets. Apart from these; jet also depends on the liner material; it's density and a proper stand off for each liner material [13]. By increasing the confinement Evans and Ubbelohde found that length of the jet remained the same but the total kinetic energy was increased. Another researcher Poole gave the idea that the detonation wave could be modified with the help of two explosives one with higher detonation velocity and the second with lower detonation velocity so that the detonation front impact almost normal to the walls of the liner. Apart from explosive casing the explosive itself plays an important role in the formation of shock wave and hence in jet formation. When the casing is weak the high explosive will give a smooth increasing blast or shock wave but when the casing is thick it will produce a strong shock wave[14].

Three Main Theories of Jet Formation

1. Intersecting Shock Waves theory of Kistiakowsky
2. Hydrodynamic Squirt Theory of Taylor and Birkhoff
3. Spalling Theory of Du Pont Company

1. Kistiakowsky's theory was grounded on the fact that when two shock waves having planer nature meet at angle greater than eighty degree, a strong plane shock is generated as a result which acts perpendicular to the bisector of the angle. Higher velocity of the jet is obtained in this way while the velocity gradient could be explained by the reduction of the detonation pressure in the region of the base of the liner where there was less explosive. This theory was unable to explain the formation of slug and jet.

2. G I Taylor presented a mathematical model of certain ideas put forward by James Tuck [15]. Tuck proposed that the high jet velocity was simply due

to hydrodynamic effects and could be explained by regarding the liner as a fluid conical shell which is given a velocity normal to the cone Tuck concluded with the help of Taylor model that explosive located in the rear axial portion of the charge was not utilized fully and progress in performance might be obtained by redistributing it towards the boundary of the liner. He also deduced that by using composite liners, jet penetration could be improved. He gave the idea of multiple coaxial jets. He included the spark photographs in his work which is considered to be the first spark photograph. Both Professor Taylor and Tuck's worked neck to neck. Taylor gave mathematical model for the thin Jet with higher velocity and the thick plug with reduced velocity. This theory was unable to explain the formation of secondary fragments and the bending back of liner. This theory was then proved with radiographs and results obtained during experiments. Taylor together with Birkhoff published their research in 1948 [16].

3. The spalling theory assumed that the inner part of the cone wall was ripped off by the spalls effect and it then travelled towards the axis where they collided to form the jet. The remaining part of the cone collapsed to form the plug. The spall theory was unable to explain the focussing of the particles and higher jet velocities.

## 2.6 Experiments and Theory of Target Penetration

Early experiments were performed to explain the mechanism of jet penetration into metals. It was considered at one stage that penetration is merely due to high temperature erosion. Evans and Ubbelohde gave the idea that when a high energy jet hits a metal target, high pressures are produced in the target which exceeds yield strength of the target and hence it behaves like a fluid. This was verified by observing the holes due to jet penetration. It was observed that almost all of the material moved radially outward from the hole and but a little moved in the direction of the hole. A lot of experiments were perfprmed to verify the deduced penetration laws. Experiments were performed on thick steel targets and spaced plates. Ubbelohde found that it was hard to penetrate the spaced steel plates instead of one thick steel plate. Reduced penetration in spaced plates was due to the

dispersion of fragments punched from the plates by the jet, which were lost in the gap between the plates. He concluded that to defeat a jet the armour plates must be spaced but the space between two plates must not be greater than one charge diameter. Hill, Mott and Pack published their work to describe the penetration laws theoretically. They considered the Evans and Ubbelohde theory of jet penetration because of very high pressures more than the yield strength of the target material. They presented a mathematical model for hydrodynamic laws governing the penetration of the jet [17]. Main points they concluded were that the penetration depth of the jet is inversely proportional to the square root of the density of the target material and is independent of the strength of the target. The penetration depth does not depend on Jet velocity. The jet length or its density should be increased in order to obtain higher penetration. When the standoff was increased penetrations was increased this was due to the fact that a more lengthy jet is obtained by increasing the standoff.

To consider the velocity distribution in jet, Pack and Evans reformed the Hill-Mott-Pack theory. There was ambiguity about the particulate nature of the jet; collected jets during experiments had very large number of small particles distributed uniformly along the jet axis. The hollow charge principle was also incorporated in gun fired projectiles. Gun fired projectile gets their aerodynamic stability by spinning which degrades the performance of jet which was a bigger problem in nineteen forties. After the WW II research on rifle grenades was almost abandoned because they could not defeat tanks and only random work was done on gun-fired munition. Area of concentrated research was wave shaping of the detonation front with the help of wave shapers and refinements in shape and material of the liner. It's filling and fabrication was also given proper attention to get reproducible penetration. Misalignment among liner, explosive and casing and uneven thickness of the liner also decreased the shaped charge performance. It was noticed that gap between the liner and explosive, density variation of the charge or porosity in charge drastically reduced the penetration. In year 1952 Taylor-Birkhoff theory was extended by Tupper to asymmetric collapse and the symmetry requirement for the collapse process was justified. UK has done a lot of work on shaped charges in the last 30 years and have developed many artillery fired shaped

charges. Most shaped charges have penetration equal to 3 to 6 cone diameter. This can be increased to 10 cone diameter in future.

## 2.7 Diagnostics Techniques

In order to investigate instabilities in jet formation, predict proper standoff distance, jet particulation and to find jet velocity mostly flash radiography is used. Flash radiography is used for weapon analysis in such a way as x- rays are used for human body. Application of flash radiography started during the Manhattan project of US in 1940. They used flash radiography technique to measure the velocity of the imploding material and the state of the metal during implosion in order to determine the optimal timing of the neutron initiators needed to achieve successful device performance. In recent times shaped charges are studied with flash radiography techniques. The machines for radiography are categorized by their power i.e. 500KeV, 650KeV or 1MeV. Following are the radiograph of molybdenum lined shaped charge with 450 KeV [18].

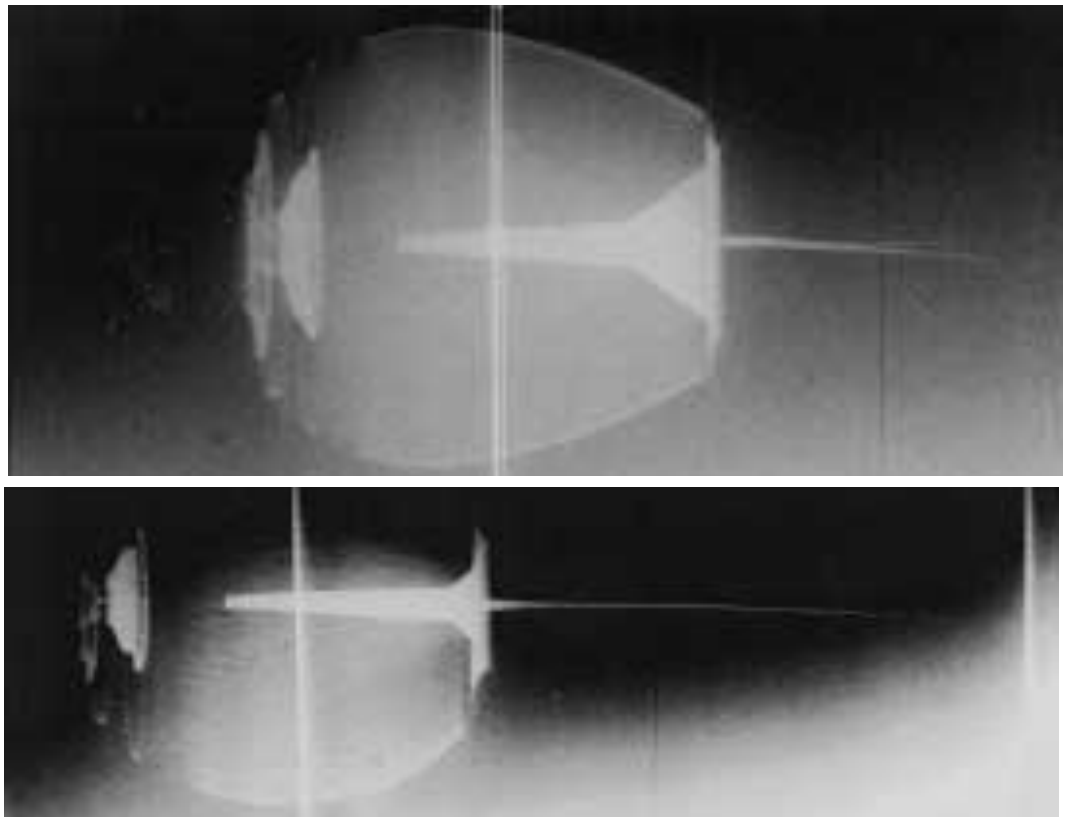

Figure 2-2 Jet Radiographs [18]

Apart from flash radiography high speed photography or streak camera is also used to study the shaped charge phenomenon [19]. It is used for finding VOD of the main charge, shock arrival time at specified locations and the symmetry of the shock wave formed during detonation [20]. A number of theories on jet penetration have been verified experimentally but a little work is being done on the radial crater growth of shaped charges. This radial crater growth phenomenon was also verified by streak camera [21].

# Shaped Charge Jet Formation Theories

## 3.1 Theory of Shaped Charge Jet Formation

Before going into detailed theory of conical shaped charge a preliminary work on the metal plates flying in contact with the explosives is presented first. It is known as Gurney Model. It gives an explicit relation for the estimation of velocity of the metal plate in contact with the detonating explosive. Gurney velocity approximation is based on conservation principles of energy and momentum. Gurney velocity approximations are within 10% of the experimental or numerical results. Gurney equation is valid over a vast range of mass to charge (M/C) ratios i.e. ($0.1 \leq M/C \leq 10$) [22].

### 3.1.1 Gurney Equations

Gurney equations are derived by the conservation of momentum and energy conservation principles. To derive Gurney equation consider Figure 3-1 sandwich of metal and explosive and Figure 3-2 which shows linear velocity distribution of explosive and metal plate.

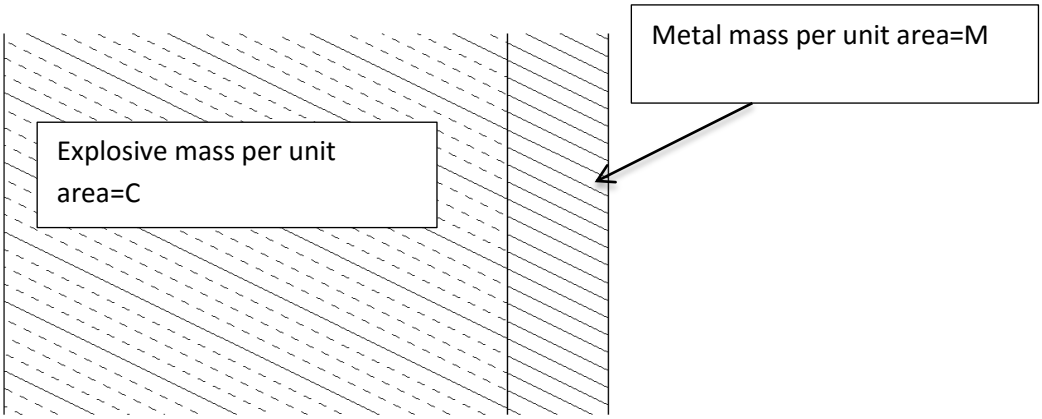


Figure 3-1 Metal and explosive in contact

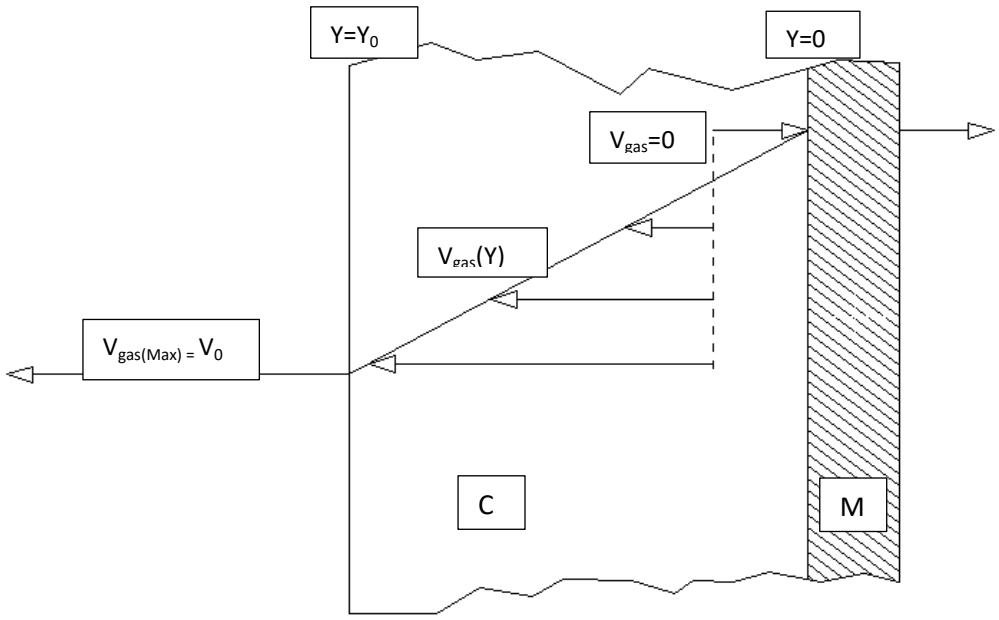


Figure 3-2 Velocity distribution for the metal explosive sandwich

Velocity distributions obtained from (Figure 3-2) is

$$V_{gas}(Y) = (V_0 + V) * \frac{Y}{Y_0} - V$$

Here V is the velocity of the flying plate, applying the momentum balance we get

$$0 = -MV + \rho_e \int_0^{Y_0} \left[ (V_0 + V) * \frac{Y}{Y_0} - V \right] dY$$

And applying the energy balance we get

$$CE = \frac{1}{2} MV^2 + \frac{1}{2} \rho_e \int_0^{Y_0} \left[ (V_0 + V) * \frac{Y}{Y_0} - V \right]^2 dY$$

Where $C=Y_0\rho_e$ and E is explosive specific kinetic energy also called gurney energy

From the above three equations we get $V_0 = V(1 + \frac{2M}{C})$

Finally we get result for V after integration and eliminating V0

$$V = \sqrt{2E}\left[\frac{\frac{4M^3}{C^3} + \frac{9M^2}{C^2} + \frac{6M}{C} + 1}{3(1 + \frac{M}{C})}\right]$$

The equation given above is applicable to the open faced sandwich as shown in Figure 3-1. Similarly equations for the velocity of flying plate for other configurations like cylinder and sphere can be obtained.

### 3.1.2 Birkhoff et al. Model

Birkhoff et al. was the first to formulate the theory for conical shaped charges. Assumption made in his theory was that detonation front creates a huge amount of pressure over the liner material such that strength of liner can be ignored. The liner instead of solid is taken as incompressible and inviscid fluid. More over the conical shaped liner was taken as wedge for modelling. A steady state collapse of the cone results in the formation of jet whose length is equal to the slant height of cone. It was observed that jet itself has some velocity gradient along its length which was not considered in Birkhoff et al. model. Jet's tip moves faster than segment just behind it and its tail has a lowest velocity which contributes to the slug. In other words we can say that the jet is continuously being pulled from behind. As a result of this gradient, jet is stretched and finally it breaks or particulation starts. The model was modified by Pugh et al. to include the velocity gradient. He considered that the collapse velocity of all the liner elements is not the same, but it depends on the initial position of the element in the liner.

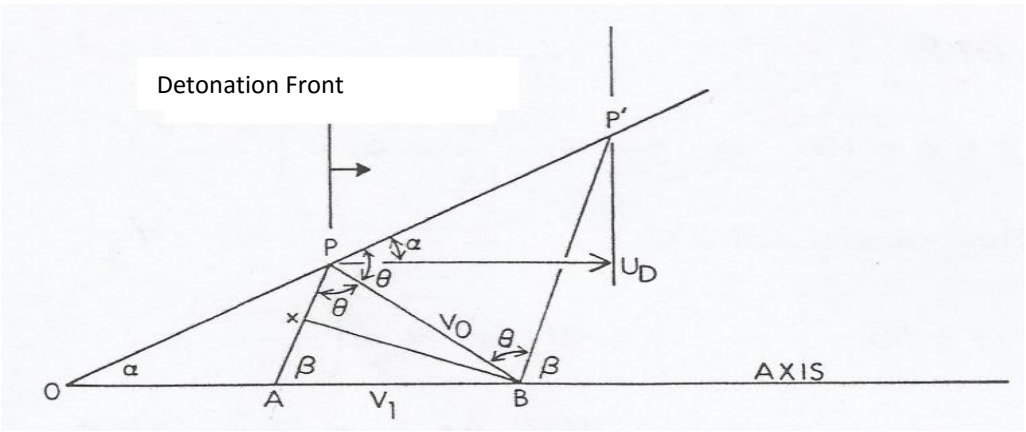


Figure 3-3 Collapse model geometry for birkhoff et al. model [23]

By the conservation of momentum and using trigonometry we get the formulae for the masses and velocities of jet and slug respectively as follows [22].

$$m_j = \frac{1}{2}m(1 - cos\beta) \qquad\qquad m_s = \frac{1}{2}m(1 + cos\beta)$$

$$V = V_0[\frac{Cos\left(\frac{\beta - \alpha}{2}\right)}{Sin\beta} + \frac{Cos\left(\frac{\beta - \alpha}{2}\right)}{tan\beta} + \sin\left(\frac{\beta - \alpha}{2}\right)]$$

$$V_s = V_0[\frac{Cos\left(\frac{\beta - \alpha}{2}\right)}{Sin\beta} - \frac{Cos\left(\frac{\beta - \alpha}{2}\right)}{tan\beta} - \sin\left(\frac{\beta - \alpha}{2}\right)]$$

### 3.1.3 PER THEORY

The basic criterion of the PER theory is that it considers the variable collapse velocity of the liner. This significantly improves the results obtained from steady state theory. Collapse velocity at the apex is greater and it gradually decreases towards the base of the cone. It is illustrated in Figure 3-4.

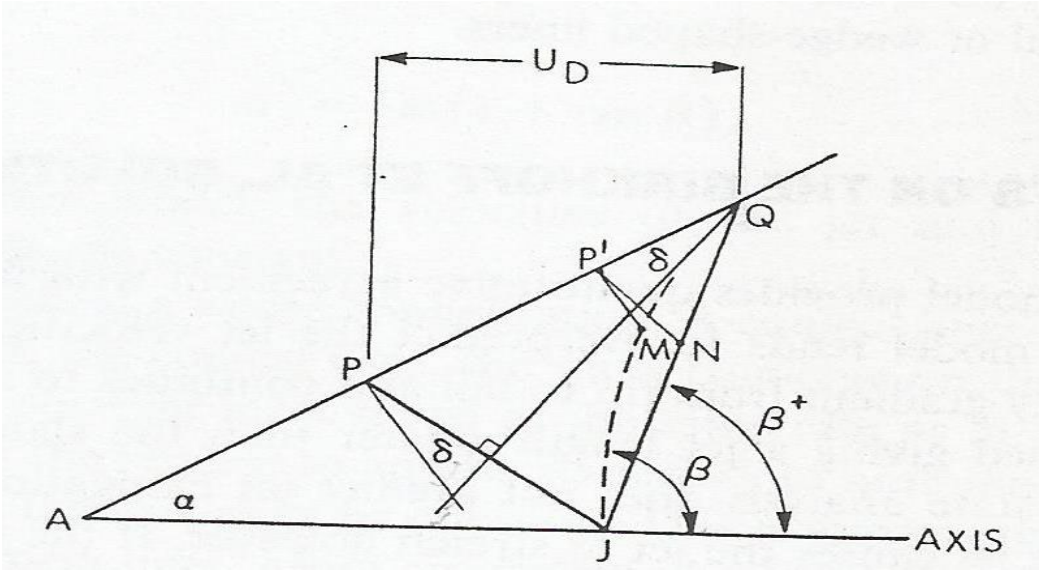


Figure 3-4 Liner Collapse Process For Variable Element Velocity [23]

Considering two elements of the liner which were at P and P` initially, as the detonation wave passes through the points APQ the liner element at P and P` moves to the points J and M respectively. If the collapse velocity of the liner elements were identical they would reach at points J and N. For equal element velocities the liner surface will remain conical or in other words the line joining

points Q,N and J i.e. QNJ will be a straight line and for variable element velocities the liner surface will not remain straight and the collapsing pattern is depicted by the line QMJ. The angle (β+) formed by the assumption of constant element velocity is smaller than the angle formed (β) by the assumption of variable element velocity. This shows that each individual liner element is not affected by its neighbour elements, which is in agreement with the hydrodynamic assumption.

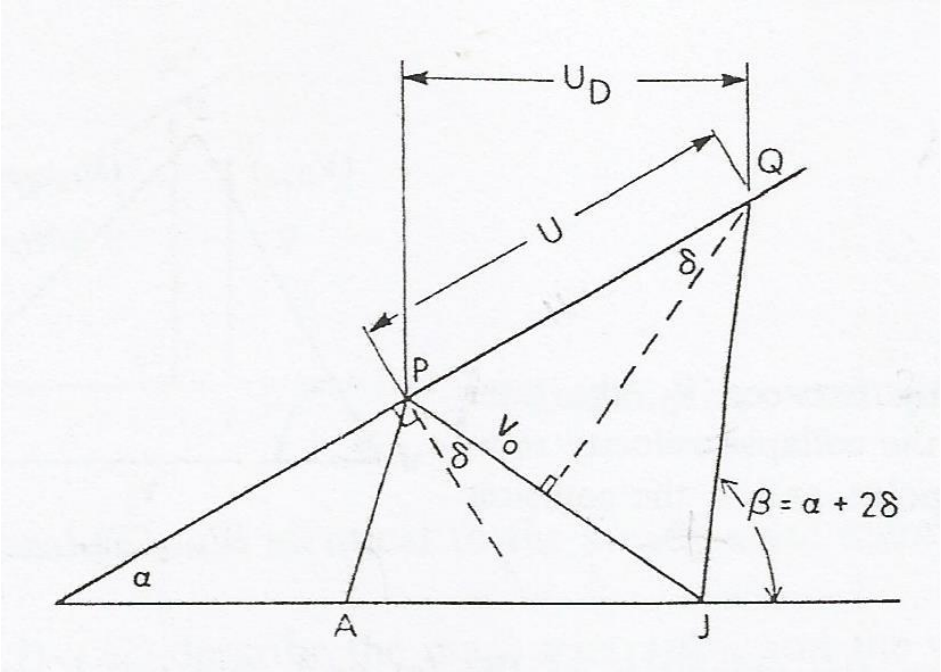


Figure 3-5 Velocities of the liner element [23]

From Figure 3-5it is clear that QJ is equal to QP in magnitude and parallel to PA. Taking |QJ|=|QP|=U, then U represent the velocity in Lagrangian or moving coordinate system of the liner element at point P. in Eulerian or laboratory or stationary coordinate system velocity of the liner element at point P is V0. The liner element does not move at 90 degree to its original position but makes a small angle δ with the normal. From figure we get that

$$\sin\delta = \frac{V_0}{2U}$$

If $V_0$ remain constant then both the angle β and β+ in Figure 3-4 will be equal and δ=(β-α)/2 we get the same results as obtained by the constant velocity model [22].

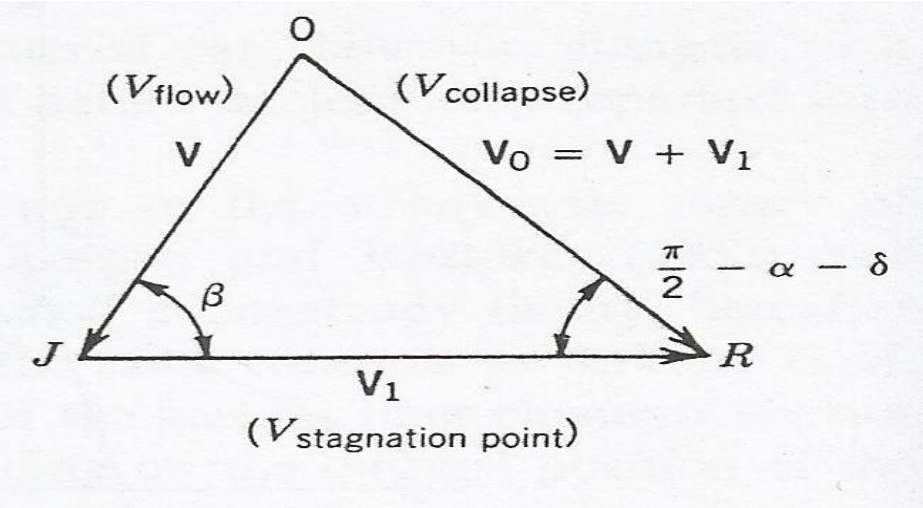


Figure 3-6 Graphical representation of the relationship between V,V1 and V0 [23]

Here V is the collapse velocity with respect to the collision point, V1 is the velocity of point of collision and V0 is the collapse velocity of the liner. JR is the axis of the collapsing cone; OJ is the collapsing element whose velocity is V in Lagrangian coordinate system where velocity of the Lagrangian coordinate system itself is V1. Applying the law of sines to Figure 3-6 we get

$$V = \frac{V_0 \cos(\alpha + \beta)}{sin\beta} \qquad \text{Eq. 3-1}$$

and

$$V_1 = \frac{V_0 \cos(\beta - \alpha - \delta)}{sin\beta} \qquad \text{Eq. 3-2}$$

In Eulerian coordinate system velocity of the slug and jet are given by the relations

$$\mathrm{Vs} = \mathrm{V1} - \mathrm{V} \qquad \text{Eq. 3-3}$$

And

$$\mathrm{Vj} = \mathrm{V1} + \mathrm{V} \qquad \text{Eq. 3-4}$$

Combining equations Eq. 3-1 to Eq. 3-4 we get the following relations for the velocities of the slug and the jet during shaped charge formation process according to PER theory.

$$V_s = V_0 sec\frac{\beta}{2}\sin\left(\alpha + \delta - \frac{\beta}{2}\right) \quad \text{Eq. 3-5}$$

And

$$V_j = V_0 csc\frac{\beta}{2}\cos\left(\alpha + \delta - \frac{\beta}{2}\right) \quad \text{Eq. 3-6}$$

By putting $\beta=\beta^+$ which is equal to $\alpha+2\delta$ according to Figure 3-5 these equations then reduces to the equations of Birkhoff et al. By eliminating $\delta$ from Eq. 3-5 and Eq. 3-6 we get.

$$V_s = V_0 sec\frac{\beta}{2}\sin\left(\alpha + sin^{-1}\frac{V_0}{2U} - \frac{\beta}{2}\right) \quad \text{Eq. 3-7}$$

$$V_j = V_0 csc\frac{\beta}{2}\cos(\alpha + sin^{-1}\frac{V_0}{2U} - \frac{\beta}{2}) \quad \text{Eq. 3-8}$$

These equations only tell the velocities of the jet and the slug, we must need to find the masses of the slug and jet. Masses can be obtained by the conservation of mass and momentum.

$$\frac{dm_j}{dm} = sin^2\frac{\beta}{2} \quad \text{Eq. 3-9}$$

And

$$\frac{dm_s}{dm} = cos^2\frac{\beta}{2} \quad \text{Eq. 3-10}$$

PER theory provides the information about the $V_s$,$V_j$, $\delta$, $\beta$, $m_s$ and $m_j$, but the number of unknowns are more than the equations. Experimental verification of the PER theory was carried out by Pugh and Eichelberger.

# Simulation and Experimental Results

ANSYS AUTODYN® is used for the simulation the present problem. ANSYS AUTODYN® is built to handle the nonlinear behaviour of fluids and structures in an easy and simplified way. It can be coupled with a number of CAD software like CATIA and Pro Engineer. It can import different CAD file formats like iges, dwg and prt. AUTODYN ® can directly import mesh from various soft wares like TRUEGRID® by XYZ Scientific Applications, Inc. Hypermesh and LS Dyna. It can be used in serial and parallel computation on shared memory and distributed memory systems.

ANSYS AUTODYN® has been used in the world renowned projects. For example to design the shielding system for the International Space Station, optimizing passive and reactive armour systems, modelling the World Trade Centre's impact and structural collapse in forensic investigations and other type of impact like asteroid impact on earth, vulnerability of personnel carriers to mines. It can also be used for the hypervelocity impact studies. A pictorial representation of steps involved in simulation is given in Figure 4-1 Passive armour system consists of new advanced material such as Ballistal® by IBD or it may be a multi layered composite, which is lightweight. The multi layered composite system is effective against both the kinetic energy penetrator and shaped charges [24]. The Reactive system consist of ERA (explosive reactive armour) [25].

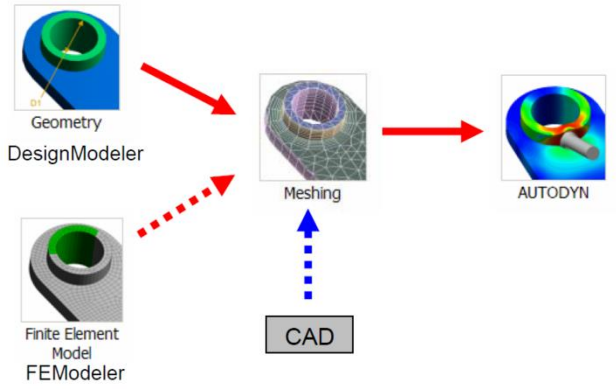


Figure 4-1 Lay out of simulation steps [26]

## *4.1 Material Properties.*

Materials used for the simulation of shaped charge are copper, Perspex, HMX, tetryl and aluminium. Equation of state, strength model and other material properties of these materials are given below in tabulated form. It is to be noted that all the material data is taken from the AUTODYN® material library except that of HMX for which changes in few values like density, VOD and sound speed are carried out on the basis of experimental data.

Table 4-1 Properties of ALUMINIUM [27]

| | |
|---|---|
| Equation of State | Shock |
| Reference density | 2.78500E+00 (g/cm3 ) |
| Gruneisen coefficient | 2.00000E+00 (none ) |
| Parameter C1 | 5.32800E+03 (m/s ) |
| Parameter S1 | 1.33800E+00 (none ) |
| Parameter Quadratic S2 | 0.00000E+00 (s/m ) |
| Relative volume, VE/V0 | 0.00000E+00 (none ) |
| Relative volume, VB/V0 | 0.00000E+00 (none ) |
| Parameter C2 | 0.00000E+00 (m/s ) |
| Parameter S2 | 0.00000E+00 (none ) |
| Reference Temperature | 0.00000E+00 (K ) |
| Specific Heat | 0.00000E+00 (J/kgK ) |
| Thermal Conductivity | 0.00000E+00 (J/mKs ) |

Table 4-2 Properties of PLEXIGLAS/PERSPEX [27]

| Equation of State | Shock |
|---|---|
| Reference density | 1.18600E+00 (g/cm3 ) |
| Gruneisen coefficient | 9.70000E-01 (none ) |
| Parameter C1 | 2.59800E+03 (m/s ) |
| Parameter S1 | 1.51600E+00 (none ) |
| Parameter Quadratic S2 | 0.00000E+00 (s/m ) |
| Relative volume, VE/V0 | 0.00000E+00 (none ) |
| Relative volume, VB/V0 | 0.00000E+00 (none ) |
| Parameter C2 | 0.00000E+00 (m/s ) |
| Parameter S2 | 0.00000E+00 (none ) |
| Reference Temperature | 0.00000E+00 (K ) |
| Specific Heat | 0.00000E+00 (J/kgK ) |
| Thermal Conductivity | 0.00000E+00 (J/mKs ) |

Table 4-3 Properties of TETRYL [27]

| Equation of State | JWL |
|---|---|
| Reference density | 1.73000E+00 (g/cm3 ) |
| Parameter A | 5.86830E+08 (Kpa) |
| Parameter B | 01.06710E+07 (Kpa) |
| Parameter R1 | 4.40000E+00 (none ) |
| Parameter R2 | 1.20000E+00 (none ) |

| | |
|---|---|
| Parameter W | 0.275000 (none ) |
| C-J Detonation velocity | 7.9130E+03 (m/s) |
| C-J Energy / unit volume | 8.2000E+06 ($KJ/m^3$) |
| C-J Pressure | 2.8500E+07 (KPa) |
| Burn on compression fraction | 0.00000E+00 (none ) |
| Pre-burn bulk modulus | 0.00000E+00 (kPa ) |
| Adiabatic constant | 0.00000E+00 (none ) |
| Auto-convert to Ideal Gas | Yes |

Table 4-4 Properties of HMX [27]

| | |
|---|---|
| Equation of State | Lee-Tarver |
| Reference density | 1.74000E+00 (g/cm3 ) |
| Parameter A | 7.48000E+08 (kPa ) |
| Parameter B | 1.21000E+07 (kPa ) |
| Parameter R1 | 4.50000E+00 (none ) |
| Parameter R2 | 1.10000E+00 (none ) |
| Parameter W | 3.00000E-01 (none ) |
| C-J Detonation velocity | 8.33600E+03 (m/s ) |
| C-J Energy / unit volume | 9.50000E+06 (kJ/m3 ) |
| C-J Pressure | 3.11000E+07 (kPa ) |
| Burn on compression fraction | 0.00000E+00 (none ) |
| Pre-burn bulk modulus | 0.00000E+00 (kPa ) |

| | |
|---|---|
| Adiabatic constant | 0.00000E+00 (none ) |
| Auto-convert to Ideal Gas | Yes |
| Reaction zone width | 2.50000 |
| Max change in reaction ratio | 0.10000 |
| Ignition parameter I | 44.0000 |
| Ignition reaction ratio exp. | 0.22200 |
| Ignition critical compression | 0.00000 |
| Ignition compression exp. | 4.00000 |
| Growth parameter G1 | 0.00000 |
| Growth parameter G2 | 1.300000e+003 |
| Growth reaction ratio exp. e | 0.222000 |
| Growth reaction ratio exp. g | 0.667000 |
| Growth pressure exp. z | 2.500000 |
| Max. reac. ratio: ignition | 0.300000 |
| Max. reac. ratio: growth G1 | 0.000000 |
| Max. reac. ratio: growth G2 | 0.000000 |
| Max. rel. vol. in tension | 1.100000 |
| Unreacted EOS | Shock |
| Gruneisen coefficient | 1.000000 |
| Parameter C1 | 0.221000 (cm/us) |
| Parameter S1 | 2.510000 (none ) |

| | |
|---|---|
| Parameter Quadratic S2 | 0.00000E+00 (us/cm ) |
| Relative volume, VE/V0 | 0.00000E+00 (none ) |
| Relative volume, VB/V0 | 0.00000E+00 (none ) |
| Parameter C2 | 0.00000E+00 (m/s ) |
| Parameter S2 | 0.00000E+00 (none ) |
| Reference Temperature | 373.0000E+00 (K ) |
| Specific Heat | 0.00000E+00 (J/kgK ) |

## 4.2 Mesh density

It is well known that a small increase in model complexity usually lead to a large increase in computational time [28]. So the computational grid size must be optimized to get accurate and quick enough results with minimum computational efforts. Various grid densities like $1mm^2$=1x1 grid lines, $1mm^2$=1.5x1.5 grid lines, $1mm^2$=2x2, $1mm^2$=2.5x2.5 grid lines and 1mm2=3X3 grid lines varying from coarse to fine were practiced. It was observed that simulation results obtained with grid density of $1mm^2$=2.5x2.5 grid lines do matches with experimental results. Therefore Ansys Autodyn® simulations were run on $1mm^2$=2.5x2.5 grid lines for optimum performance.

## 4.3 Simulations of the Experiments

Using the above mentioned materials simulations were setup in Autodyn 2D Euler solver. Units used for the simulations were cm, g and micro seconds and the symmetry was 2D- Axial, this unit seems somewhat awkward but it was the requirement of Lee and Tarver equation of state used for high explosive. Boundary was set up on the extremes of X axis and on the top in such a way that no material bounces back of the boundary while there is perfect reflection on the Y=0 because of the axial symmetry. Simulation end time was set to 30 micro second while the whole process took only 23 micro seconds to complete so the execution was

stopped earlier. Gauges were put at the required positions where slits on the mask were machined as shown in the following figures.

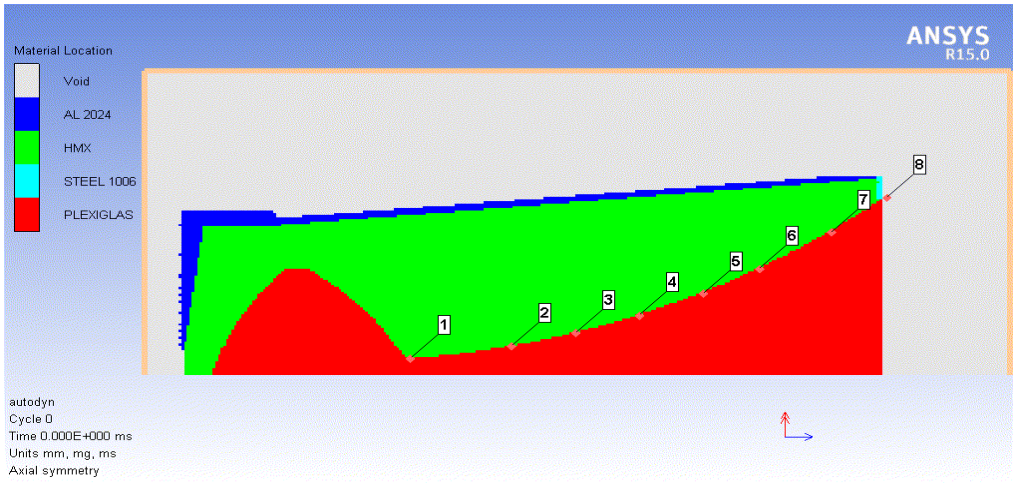


Figure 4-2 Gauges point on perspex cone ahead of wave shaper

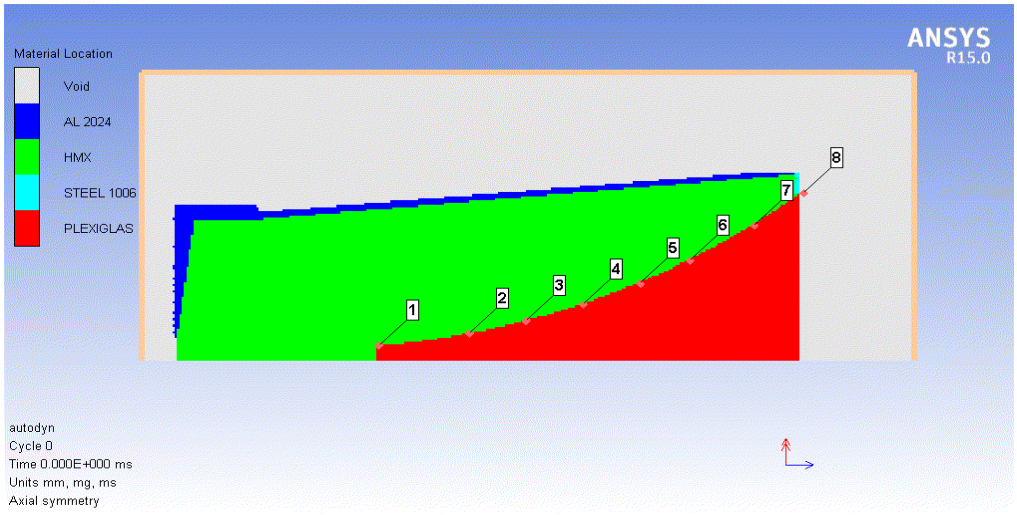


Figure 4-3 Guges point on the exterior of perspex cone without wave shaper

Comparison of both the simulations can best understood with the help of following figures. Upper side of the all the figures given below consist of simulations without wave shaper while on the lower side are those having wave shaper. Capturing times was kept the same for comparison purposes.

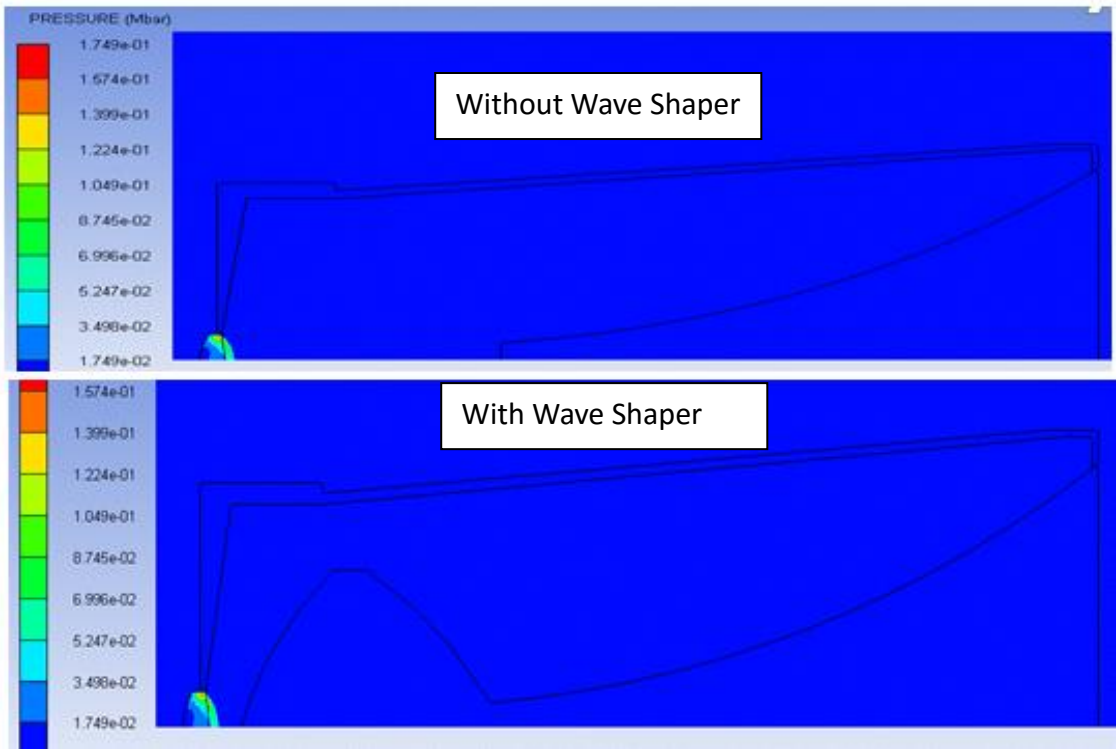


Figure 4-4 Comparison of two simulations at t=1 µsec

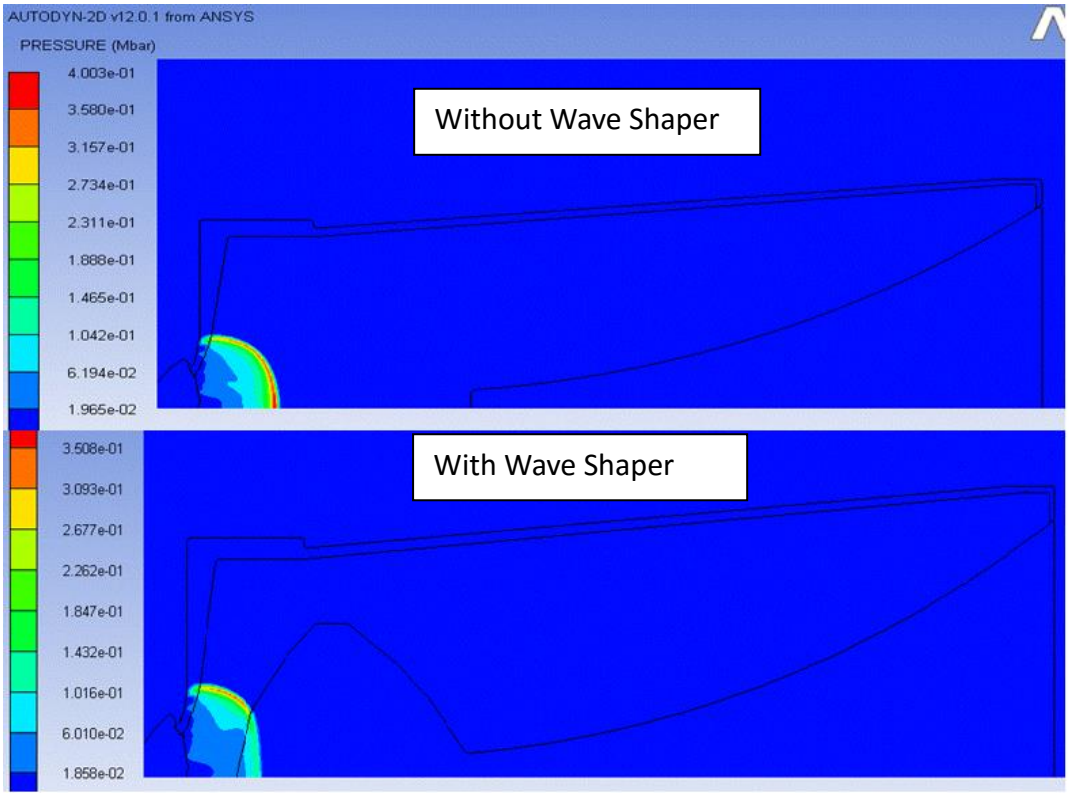


Figure 4-5 Comparison of two simulations at t=3 µsec

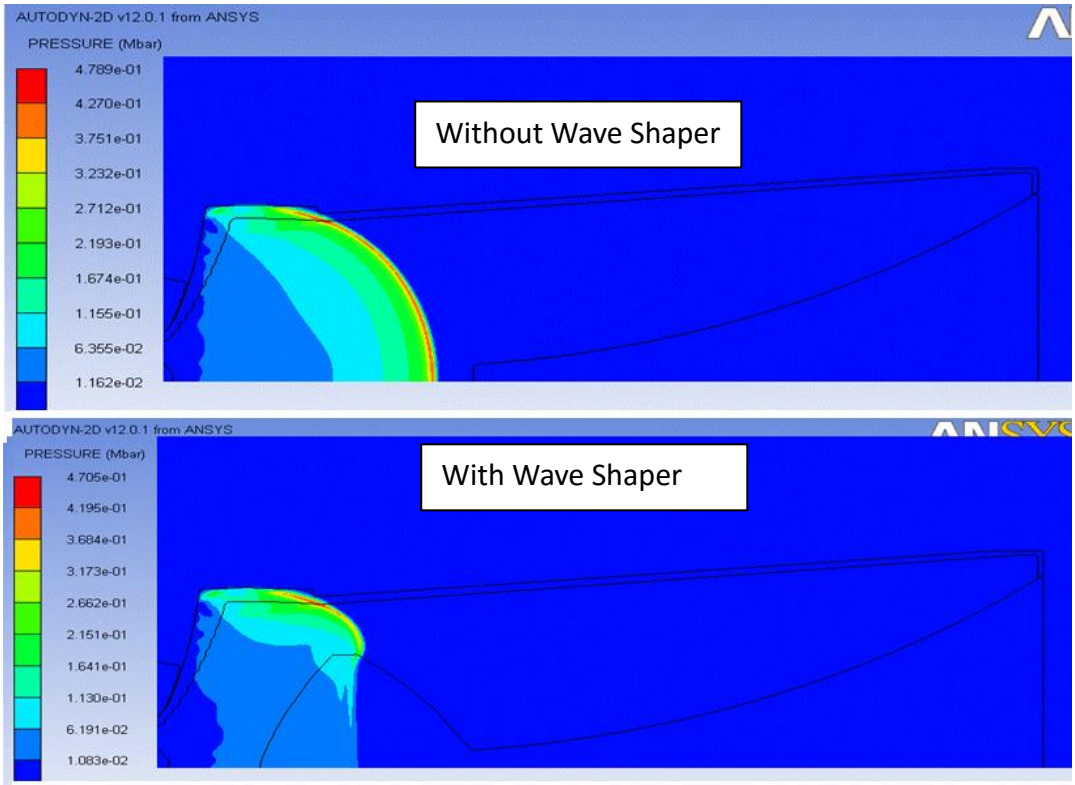


Figure 4-6 Comparison of two simulations at t=7 µsec

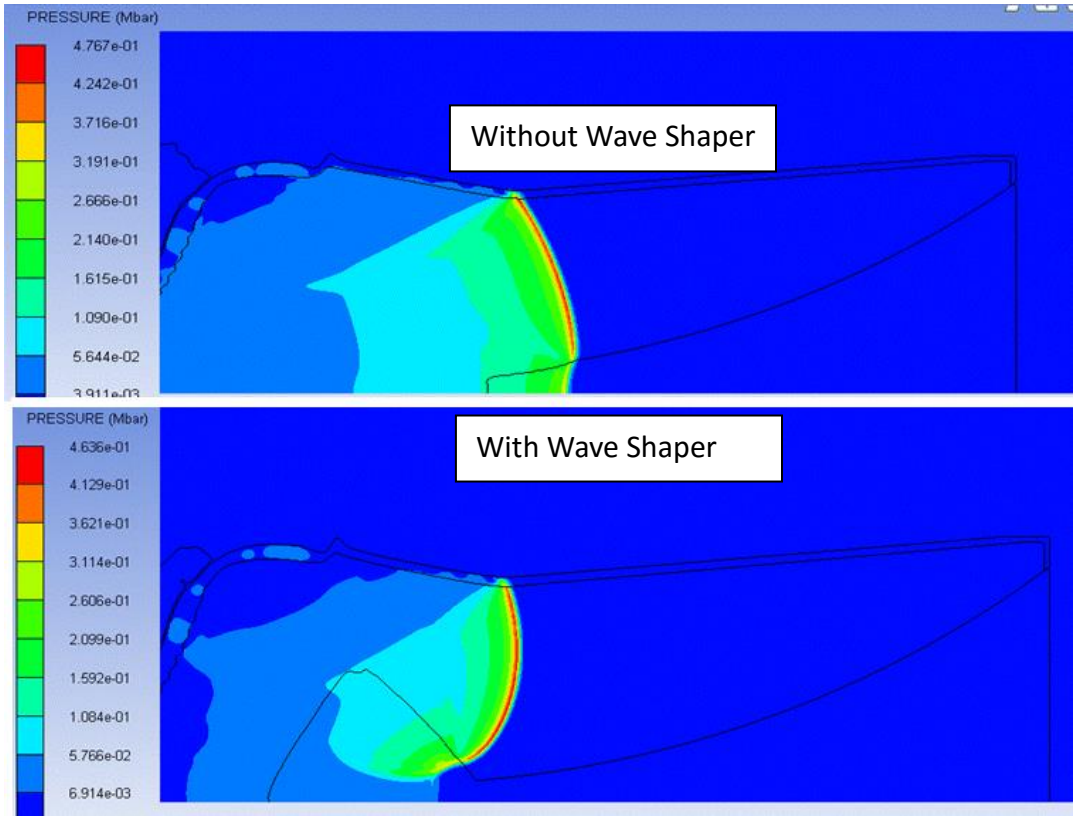


Figure 4-7 Comparison of two simulations at t=11 µsec

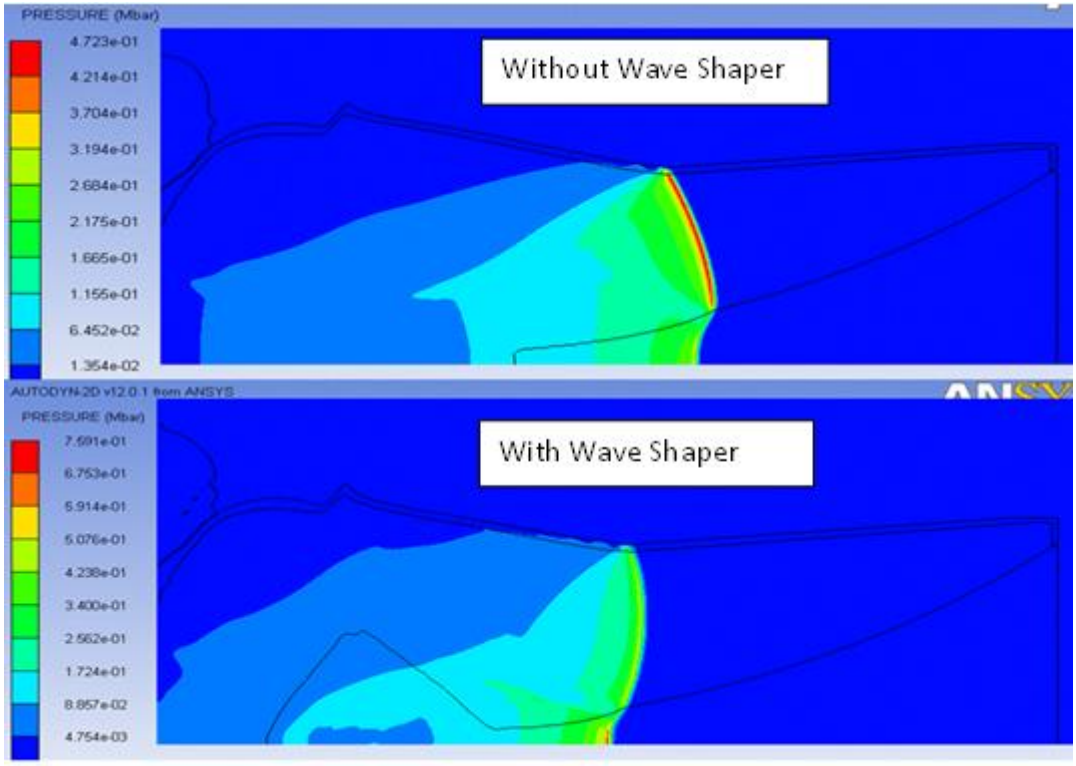


Figure 4-8 Comparison of two simulations at t=14 µsec

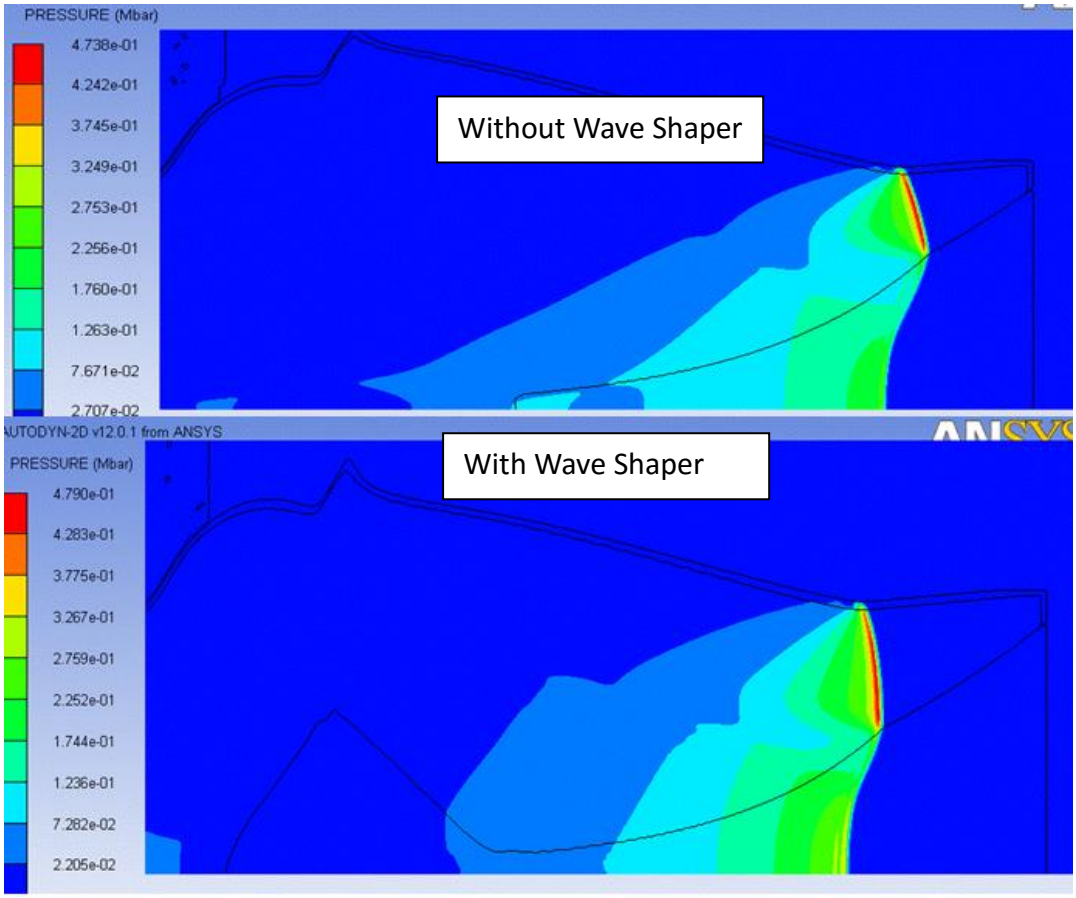


Figure 4-9 Comparison of two simulations at t=20 µsec

Figure 4-4 shows that the detonation has just started and has yet not reached the wave shaper therefore the shape of the shock front is almost identical at 1 µs. As the time passes the shock front enter the wave shaper and is impeded by it while in simulation without wave shaper the shock front is spreading in a normal way and this difference can be seen very clearly from Figure 4-5 which is captured at 3 µs. This difference increases with time and can be observed at 7 µs from Figure 4-6 at 11 µs it is worth noting that the shock is arriving the perspex mask from top in simulation with wave shaper. This top attack is required to produce a fine and high velocity jet. Thus perspex wave shaper is performing well as a wave shaper. In later times when the shock front has travelled half of the mask length in the simulation having wave shaper; its shape resemble to the shock front having no wave shaper. But the arrival time are much different. The shock without wave shaper quickly reaches the end of the explosive but the shock front in case of wave

shaper reaches one micro second later at the end because it has to turn around the wave shaper on its way.

## 4.4 Simulation Timings

Timings for the streaks to appear were taken by putting fixed gauges at specified locations on the copper cone. Gauges not only give arrival time of the shock wave, it also gives us the time history of pressure, effective plastic strain, X velocity, Y velocity, material compression and absolute velocity. Another advantage of simulation over experiment is that we can put any number of gauges at any place of our interest while in an experimental setup we can put limited number of gauges at only allowable locations. A number of gauges were put during both the simulations to find various aspect of the setup at positions, as shown in Table 4-5.

Table 4-5 Gauge coordinates

| **Gauge Number** | **Position in XY Space** | |
|---|---|---|
| | **X** | **Y** |
| 01 | 57.60 | 4.83 |
| 02 | 83.25 | 8.50 |
| 03 | 99.50 | 12.40 |
| 04 | 115.75 | 17.60 |
| 05 | 132.00 | 24.00 |
| 06 | 146.25 | 31.23 |
| 07 | 164.50 | 42.18 |
| 08 | 178.60 | 52.35 |

Shock arrival timings observed by simulations are given in Table 4-7. These timings are noted at peak pressures observed on desired locations over the pespex mask.

Table 4-7 Simulation timings

| Gauge Number | Shock Arrival Time (μs) | |
|---|---|---|
| | **Without Wave Shaper** | **With Wave Shaper** |
| 1 | 8.04 | 12.21 |
| 2 | 11.12 | 13.45 |
| 3 | 13.04 | 15.06 |
| 4 | 14.99 | 16.78 |
| 5 | 16.98 | 18.59 |
| 6 | 18.78 | 20.24 |
| 7 | 21.02 | 22.35 |
| 8 | 23.01 | 24.29 |

Table 4-8 Maximum pressure observed at the gauges

| Gauge Number | Pressure (M bar) | |
|---|---|---|
| | **Without Wave Shaper** | **With Wave Shaper** |
| 1 | 0.43060 | 0.59377 |
| 2 | 0.34399 | 0.44952 |
| 3 | 0.32278 | 0.38183 |
| 4 | 0.32543 | 0.36563 |
| 5 | 0.32160 | 0.35493 |
| 6 | 0.32432 | 0.36855 |
| 7 | 0.33566 | 0.35394 |
| 8 | 0.18238 | 0.18535 |

Pressure time history of the gauges in simulation of the charge having no wave shaper and with wave shaper are plotted below respectively in Figure 4-10 and Figure 4-11.

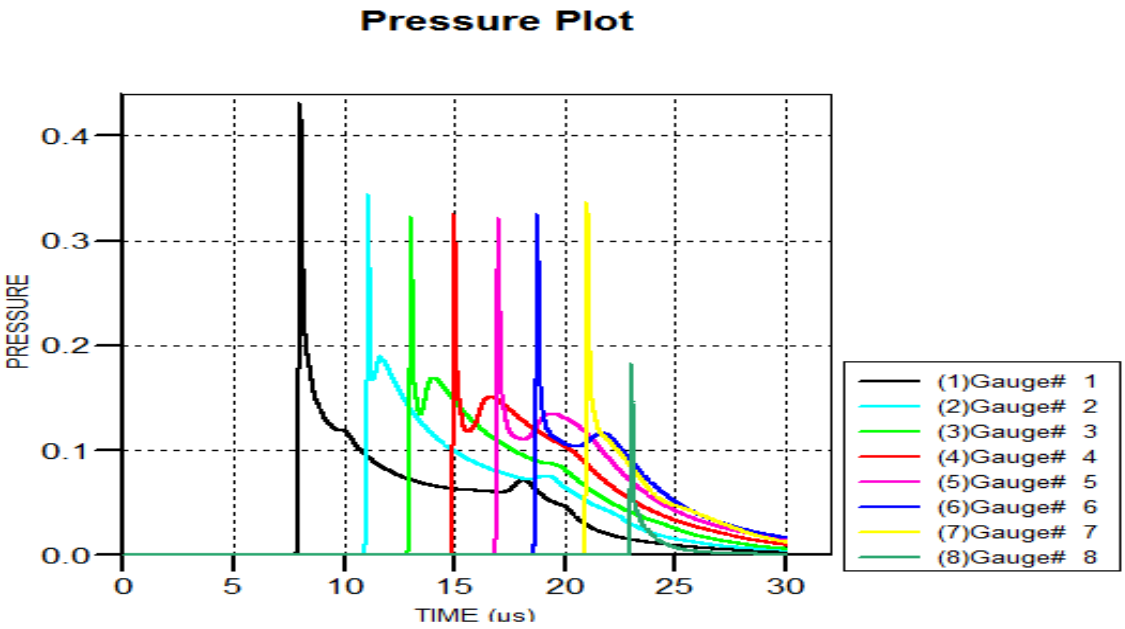


Figure 4-10 Pressure time history of gauges without shaper

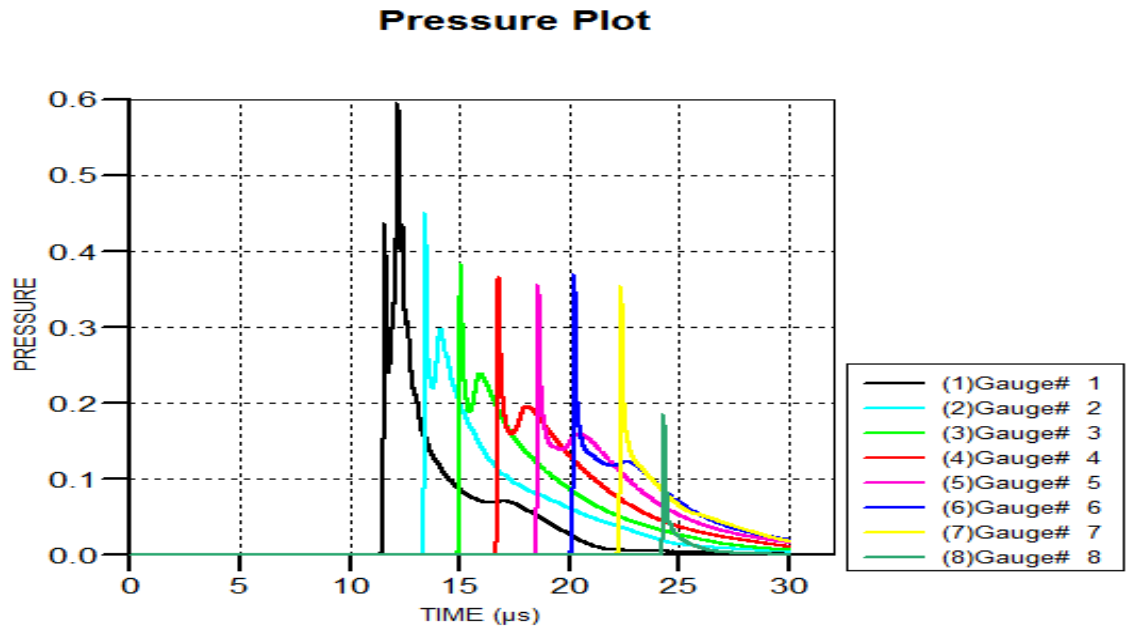


Figure 4-11 Pressure time history of gauges with wave shaper

## 4.5 Experimental setup

Perspex has the property of transmitting light under normal conditions but when it is shocked it becomes opaque. Initially manufacturing of various parts of the experiments and then experimental setup will be explained.

### 4.5.1 Perspex Mask

Perspex mask is the most important tool in capturing the streaks because of its fast shuttering speed of about 50 ns. Cone was manufactured by turning CNC machine within the required tolerance. Chuck holding part of the mask was left for turning after painting as shown in Figure 4-12. Technical drawing for machining of perspex mask is given in Figure 4-13.

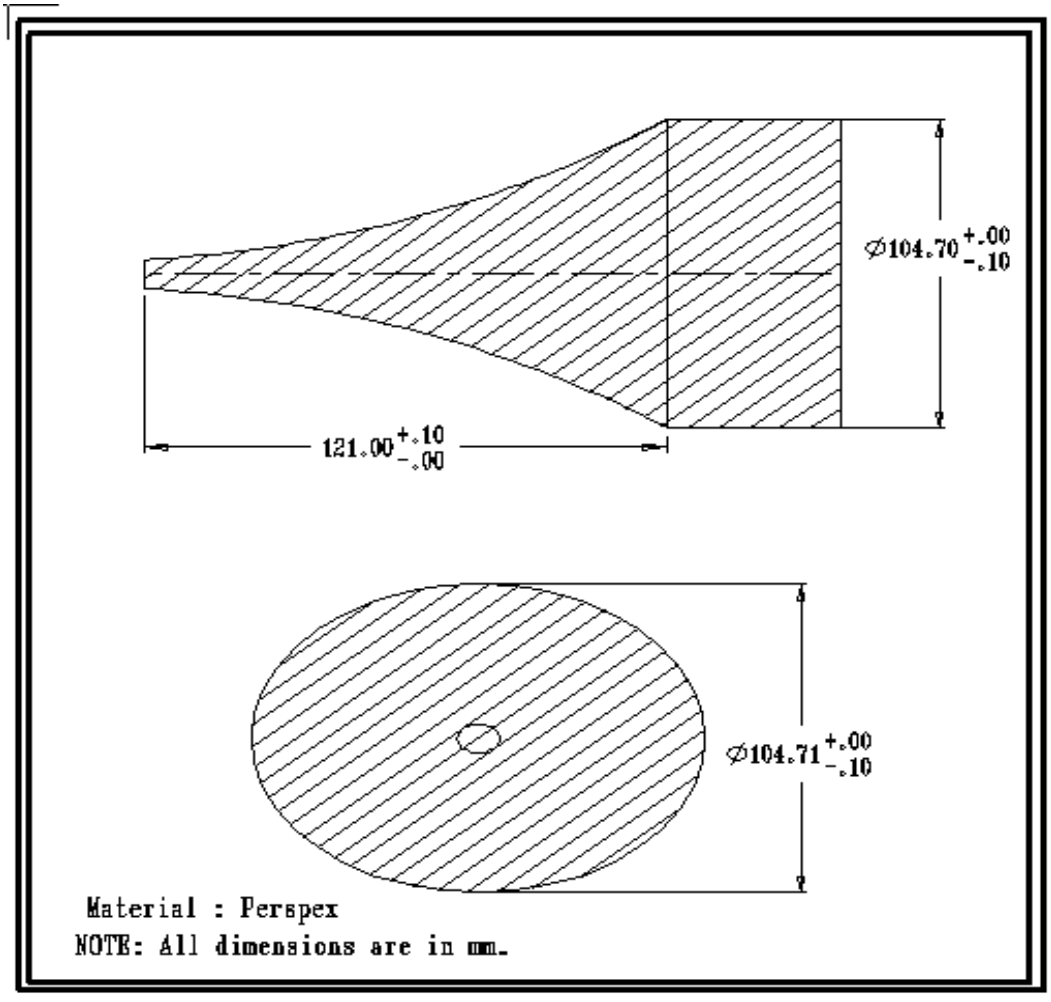


Figure 4-12 Perspex mask prior to grooves and paint

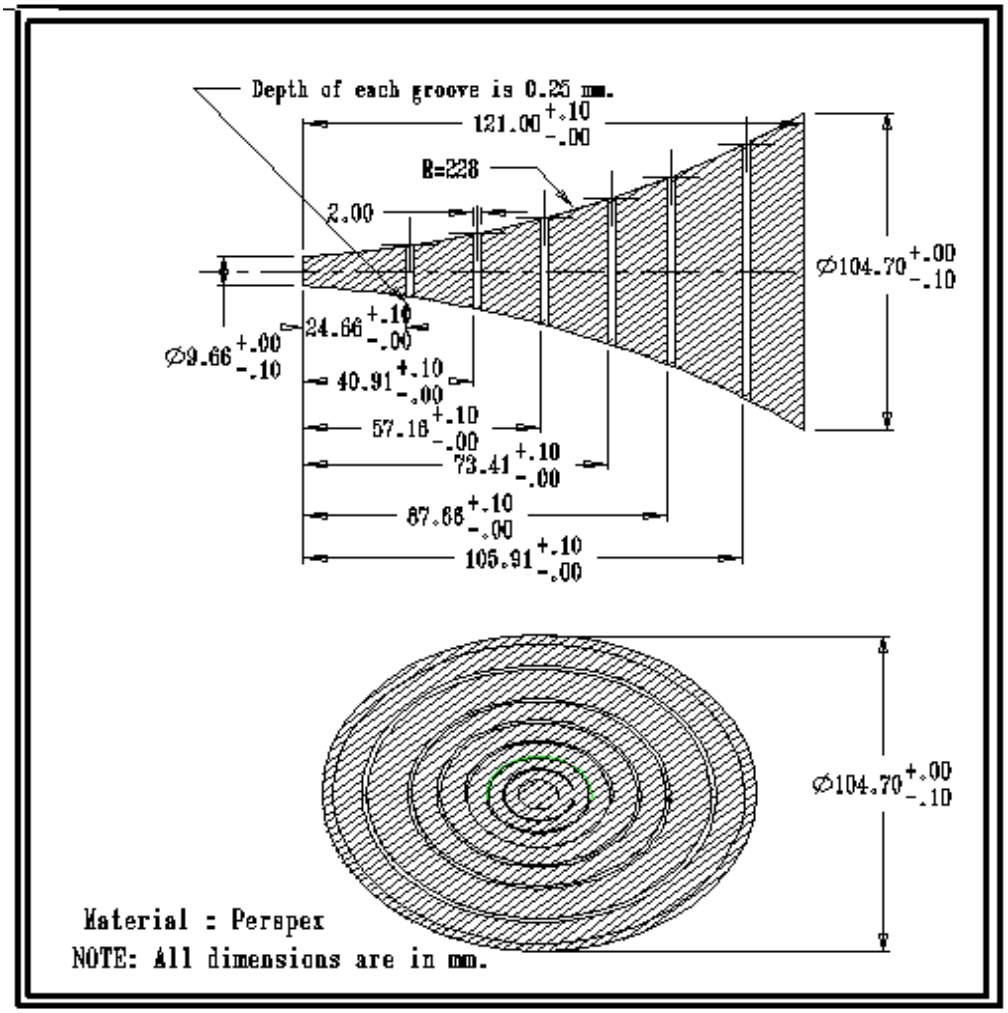


Figure 4-13 Technical drawing of the perspex mask

To make the perpxpex mask opaque it was sprayed with black paint except the base. After spraying it was observed that the thickness of the coated black paint is not uniform, so it could not be centred on lathe machine for machining of grooves. Therefore grooves were machined by milling machine and the chuck part was removed. Initially the groove depth decided was to be 0.1 mm but due to the soft nature and low melting point of perspex the depth was increased to 0.25 mm. After milling base of the cone was buffed and polished very gently so that it become transparent. Photograph of the finished Perspex cone taken from base and apex is given in. Figure 4-14.

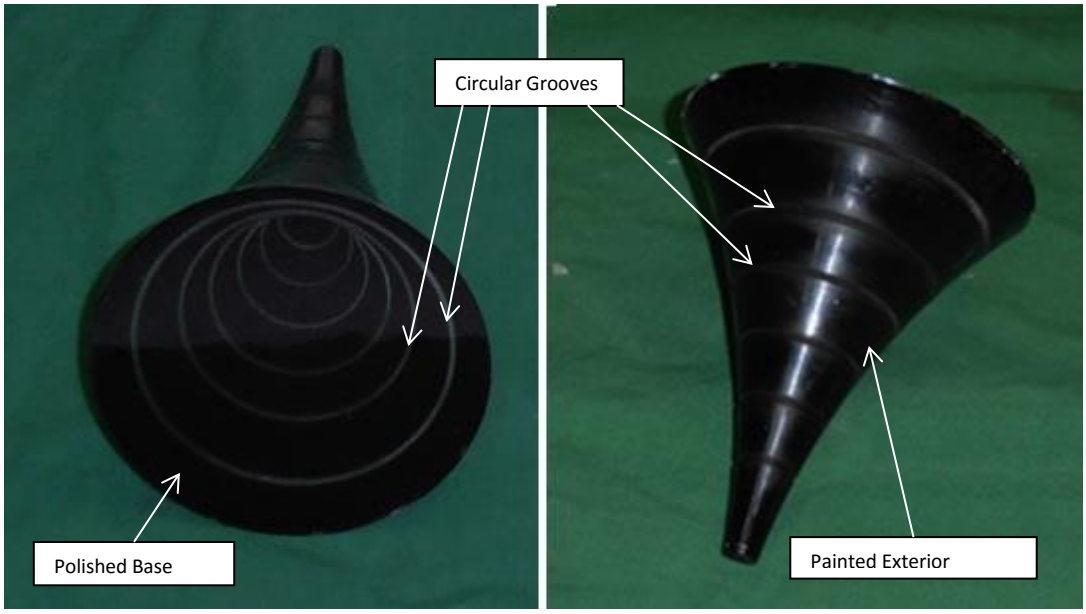


Figure 4-14 Finished perspex cone

### 4.5.2 Explosive Manufacturing.

Explosive was hydro-statically pressed and after qualification sent to machine shop where the explosive cone was manufactured within required tolerances. Machining of explosives is a dangerous work because in case of an accident no one is left to rectify the fault. Cone for the experiment with wave shaper was manufactured in two pieces in order to put the wave shaper inside the explosive and that for without wave shaper was machined in one piece. Explosive manufacturing was completed on CNC turning machines.

### 4.5.3 Casing and Other Aluminium Parts

Casing, back part and front rings of aluminium were manufactured by CNC turning machines. Four cut on the front ring and back part were machined by milling. Photograph of various parts for the experiments is given in Figure 4-15. Exploded view of the assembly is given in Figure 4-16


Figure 4-15 Individual parts of the assembly

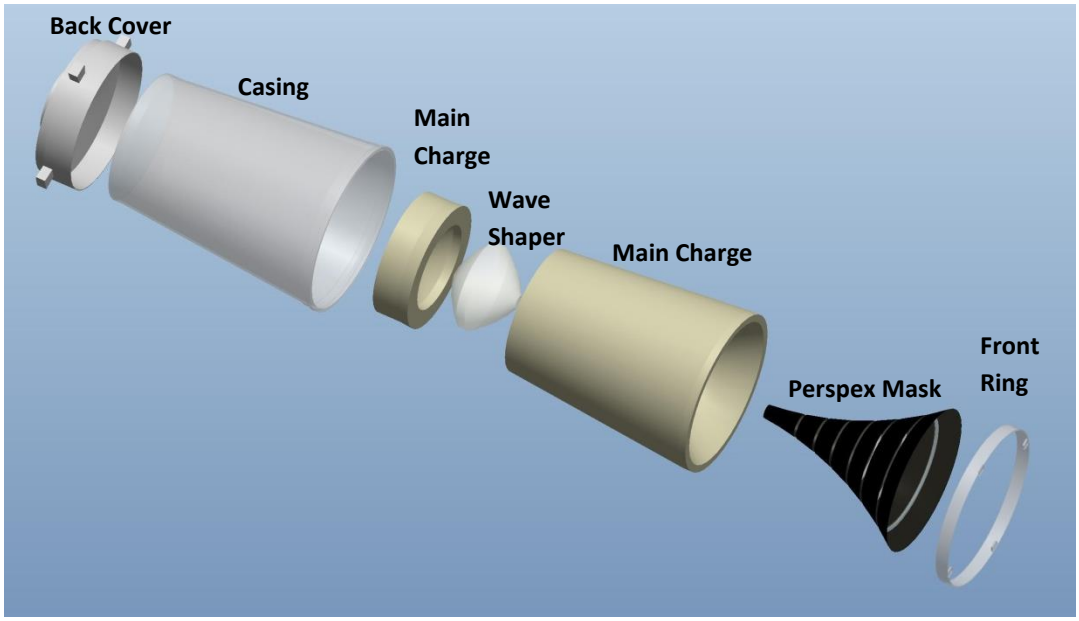


Figure 4-16 Exploded view of assembly

Assembled and ready to fire assemblies are given in

Figure 4-17 .

Figure 4-17 Assemblies with and without wave shaper

Masses of different manufactured parts are given in Table 4-7.

Table 4-6 Masses of various parts for assembly with and without wave shaper

| S.No. | Part Name | Material | Mass (Grams) | |
|---|---|---|---|---|
| | | | Without Wave Shaper | With Wave Shaper |
| 1 | Casing | Aluminium | 291.0±0.05 | 286.0±0.05 |
| 2 | Back Cover | Aluminium | 150.8±0.05 | 144.4±0.05 |
| 3 | Front Ring | Aluminium | 67.4±0.05 | 74.1±0.05 |
| 4 | Main Charge | HMX | 1995.2±0.05 | 1865.6±0.05 |
| 5 | Wave Shaper | Perspex | No Wave Shaper | 95.2±0.05 |
| 6 | Cone | Perspex | 297.50±0.01 | 296.9±0.05 |

Mass to charge ration is an important aspect of shaped charges. Mass of the copper cone used for shaped charges in both the assemblies is equal to 292.7±.05 gm. Hence mass to charge ratio in assembly I that is without wave shaper is 0.14 and for the second assembly having wave shaper in it is a bit higher because of the accommodation of wave shaper in the explosive which is 0.15. A top view of the experimental setup is presented in Figure 4-18 Assembly was put on a table in

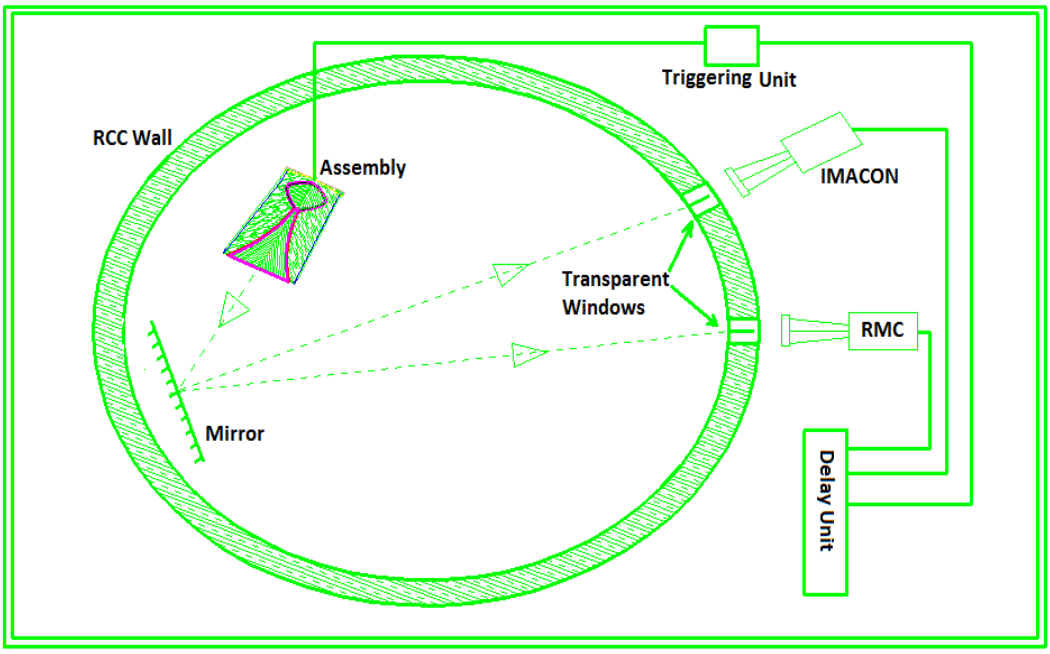


Figure 4-18 Top View of experimental setup

explosive chamber. Explosive chamber is capable to withstand blast up to 2.5 Kg of explosive. As the assembly is detonated the wave front propagates in the explosive in spherically outgoing direction. When the wave front strikes the groove of the perspex cone, air in the groove is excited to higher energy states and when it de-excites to ground state, it emits intense light. Light from these grooves passes through the cone and reaches the mirror, where it is reflected back to camera 1 and camera 2 for recording. Perspex has a unique property that it becomes opaque when shocked [20], so as the light passes from the groove it is transmitted but as soon as it is shocked by the incoming shock front perspex becomes opaque to light and acts as a shutter. These experiments are designed to exploit this property of perspex to capture the streaks. If it does not happened we would get a rectangular bright image along the whole length of the screen.

### 4.5.4 Streak Camera

Streak camera is normally called a camera but it is entirely different in mechanism from the cameras we use in daily life for still pictures and videos. Streak camera can record an ultra-fast light phenomena and delivers intensity vs. time vs position of the streak[29]. Streak camera is the best device which detects ultra-fast light phenomenon and produce temporal resolution. As it is a two dimensional device, it

can be used to detect several tens of different light channels simultaneously. For example when it is used in combination with a spectroscope, time variation of the incident light intensity with respect to wavelength can be measured. This technique is also called time resolved spectroscopy. When it is used in combination with proper optics, it is possible to measure time variation of the incident light with respect to position it is called time and space-resolved measurement.

Cameras use in the experiments to record the streaks were

1. IMACON
2. Rotating Mirror Camera (RMC)

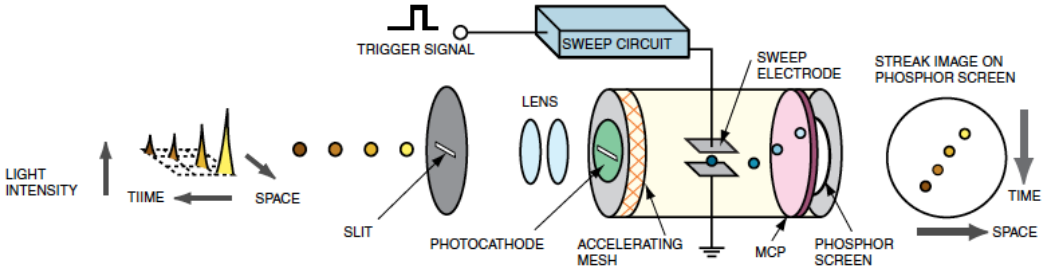


Figure 4-19 Working principles of streak tube [29]

Both the camera works on the same principles that both capture the light which is called streak. Its working principle can be understood with the help of Figure 4-19. The ultra-fast light phenomenon which is being measured in front of camera, light from the phenomenon passes through a slit or other device in this case the perspex mask on the photocathode of the streak tube. Consider four optical pulses which vary slightly in terms of both time and space, and which have different optical intensities, are input through the slit and reach at the photocathode. The incident light on the photocathode is converted into a number of electrons proportional to the intensity of the light, so that these four optical pulses are converted sequentially into electrons. These electrons then pass through a pair of accelerating plates, where they are accelerated and finally strikes a phosphor screen. As the electrons produced from the four optical pulses pass between a pair of sweep electrodes, high voltage is applied to the sweep electrodes at a time synchronized to the incident light. This initiates a high-speed sweep (the electrons are swept from top

to bottom). During the high-speed sweep, the electrons, which arrive at slightly different times, are deflected in slightly different angles in the vertical direction, and enter the MCP (micro-channel plate). As the electrons pass the MCP, they are multiplied millions of times, after which they reach the phosphor screen, where they are once again converted into visible light. On the phosphor screen, the phosphor image corresponding to the optical pulse which was the earliest to arrive is placed in the uppermost position, with the other images being arranged in sequential order from top to bottom, in other words, the vertical direction on the phosphor screen serves as the time axis. Also, the brightness of the various phosphor images is proportional to the intensity of the respective incident optical pulses. The position in the horizontal direction of the phosphor image corresponds to the horizontal location of the incident light. In this way, the streak camera can be used to convert changes in the temporal and spatial light intensity of the light being measured into an image showing the brightness distribution on the phosphor screen. We can thus find the optical intensity from the phosphor image, and the time and incident light position from the location of the phosphor image.

## 4.6 Experimental Results

Due to faults in the electronics circuitry IMACON was used only for imaging purposes and not for the data collection. All calculations are based on the streaks obtained from RMC. Slit was used in RMC while conducting experiment without wave shaper that is why we get two vertical dots along the time axis instead of rings shown in Figure 2-1. Slit was inserted because we were uncertain of the light intensity coming out of slit.

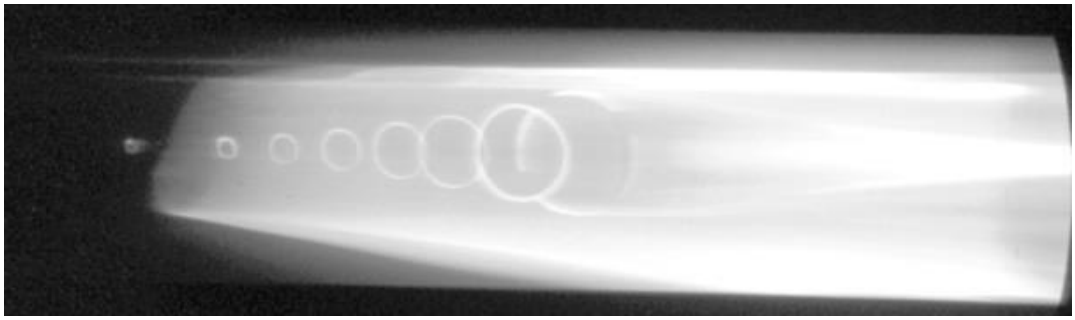

Figure 4-20 Streak obtained By IMACON for the experiment without wave shaper

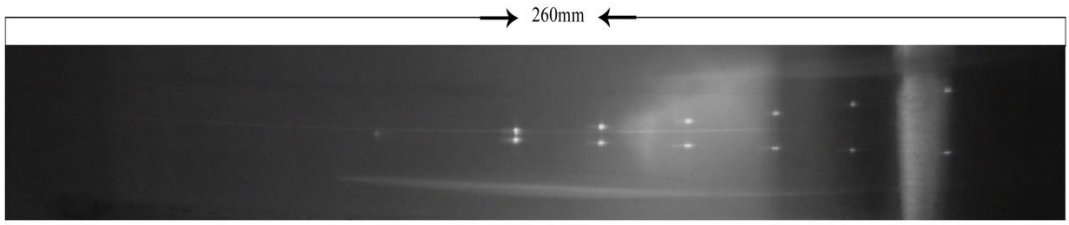


Figure 4-21 Streak obtained By RMC for the experiment without wave shaper

Distance between initial and final streak in Figure 4-21taken by the front from the apex of the cone to groove number 6 is 140mm. Speed of the film is 9mm/µsec so the time obtained by dividing the streak length with film speed is equal to 15.55 µsec while in simulation it is only 12.98 µsec. In this time shock travelled a distance of 112.08 mm measured from the technical drawing of the perspex mask. It gave shock front velocity of 7.20 mm/ µs averaged over the entire liner surface. Streak length between two adjacent spots measured from left to right are tabulated in Table 4-7 which in turn gives the times and corresponding distances are calculated from the technical drawing of the perspex mask.

Table 4-7 Streak distance and shock velocity for experiment without wave shaper

| **Experimental Times for Experiment Without Wav Shaper** | | | | | |
|---|---|---|---|---|---|
| Gauge Number | Streak Length | Time | Dist. Travelled | Shock Front Velocity | Error |
| 1-2 | $35^{+0.0}_{-0.5}$ | $3.889^{+0.000}_{-0.056}$ | 24.9 | 6403 | 093 |
| 2-3 | $22^{+0.0}_{-0.5}$ | $2.444^{+0.000}_{-0.056}$ | 16.69 | 6828 | 159 |
| 3-4 | $21^{+0.5}_{-0.0}$ | $2.333^{+0.056}_{-0.000}$ | 17.04 | 7303 | -170 |
| 4-5 | $21^{+0.5}_{-0.0}$ | $2.333^{+0.056}_{-0.000}$ | 17.5 | 7500 | -174 |
| 5-6 | $19^{+0.5}_{-0.0}$ | $2.111^{+0.056}_{-0.000}$ | 15.86 | 7513 | -193 |
| 6-7 | $24^{+0.0}_{-0.5}$ | $2.667^{+0.000}_{-0.056}$ | 21.22 | 7958 | 169 |

Plot of Shock front velocity at specified locations on the mask surface is presented in graphical form in Figure 4-22

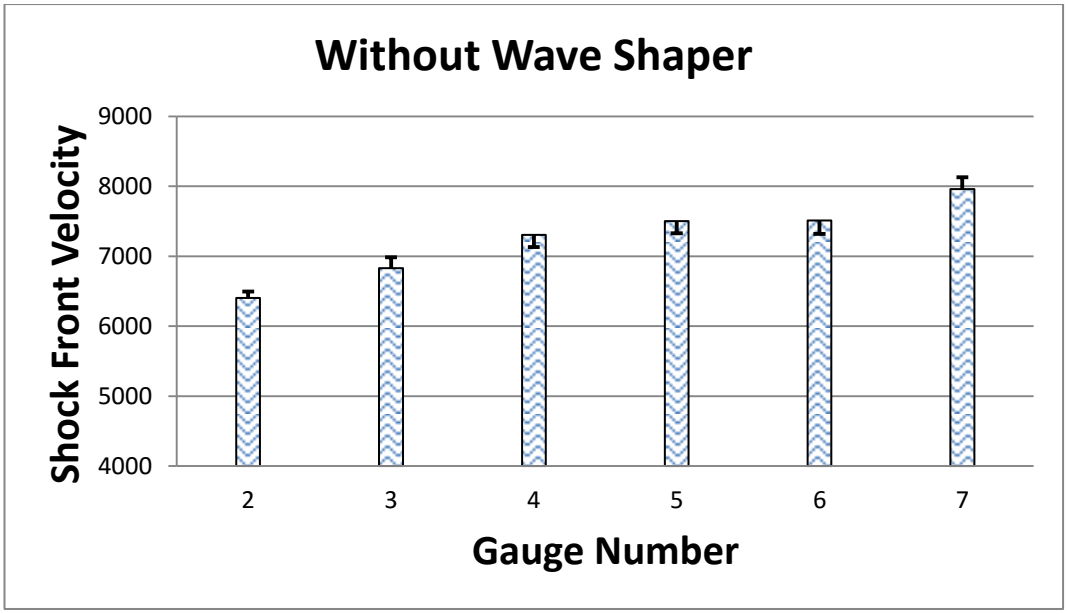


Figure 4-22 Experimental shock front velocities

To find shock front velocity from simulation the peak pressure times were observed on specified locations where fixed gauge points were put in for this purpose. These timings from simulation are given in Table 4-8

Table 4-8 Shock arrival time and velocities from simulation without wave shaper

| Gauge Number | Shock Arrival Time | Simulation Data | | |
|---|---|---|---|---|
| 1 | 8.04 | Time Diff.(μs) | Dist. Travelled (mm) | Shock front velocity (m/s) |
| 2 | 11.11 | 3.07 | 24.90 | 8111 |
| 3 | 13.04 | 1.93 | 16.69 | 8648 |
| 4 | 14.99 | 1.95 | 17.04 | 8738 |
| 5 | 16.98 | 1.99 | 17.50 | 8794 |
| 6 | 18.78 | 1.8 | 15.86 | 8811 |
| 7 | 21.01 | 2.23 | 21.22 | 9516 |

Plot of simulated shock front velocity at different locations on the mask surface is given in Figure 4-23

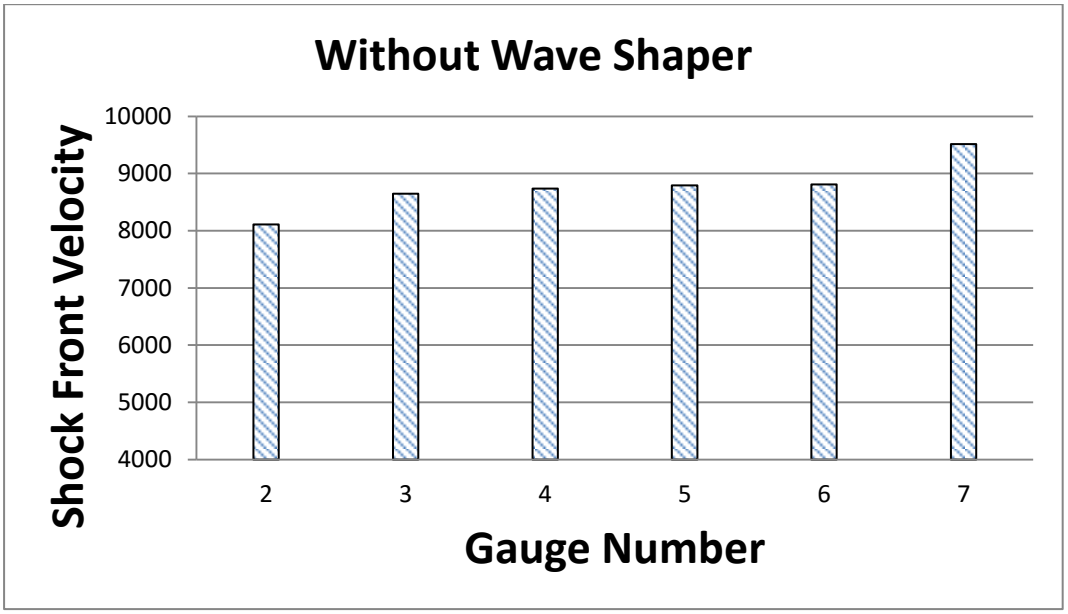


Figure 4-23 Shock front velocity from Simulation

Comparison of the experimental and simulation data timings is plotted in

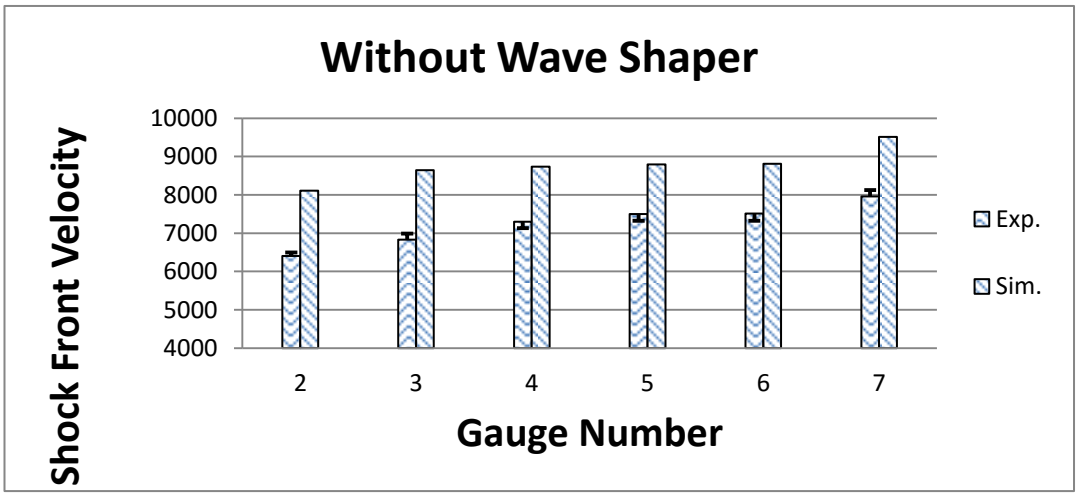


Figure 4-24 . It shows that the experimental values are lower than their corresponding simulation values.

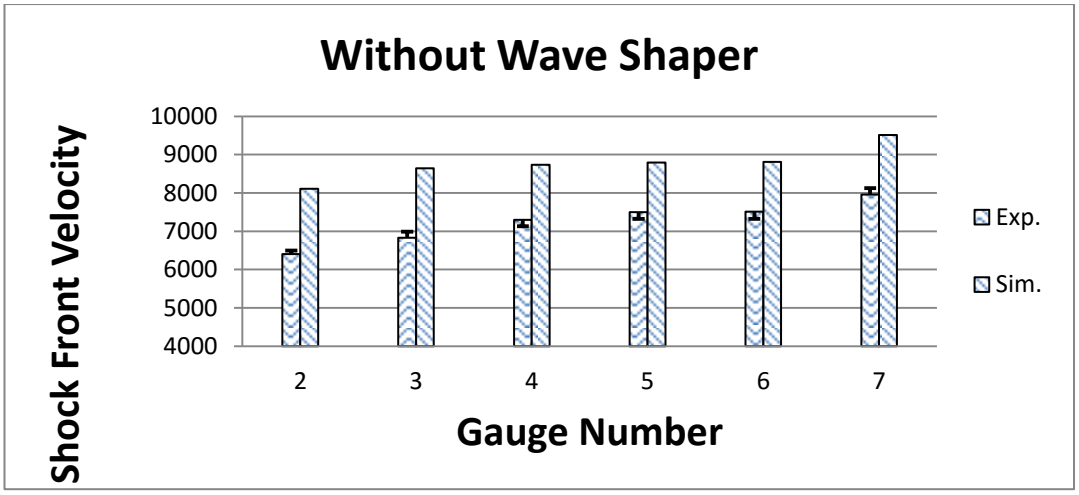


Figure 4-24 Comparison of simulation and experimental shock front velocities

The time taken from first groove to last groove in experiment having wave shaper is measured by the distance which is equal to 91+1 mm and the camera scanning speed is 9mm/µ sec which belongs to a time of 10.11+0.11 µsec, while in simulation this time is between gauge number two and seven which is 8.9 µsec. From streak data shock during 10.13 µsec travels a distance of 88.31 mm over the mask so average shock front velocity over the entire surface of the mask is equal to 8639+95 m/s while the aggregate shock front velocity calculated from simulation is 9922 m/s. Here once again the experimental results are on the lower side because there are losses and imperfections in the experiment as compared to simulations, which consider ideal case that is without any imperfections in assembly and without any side losses.

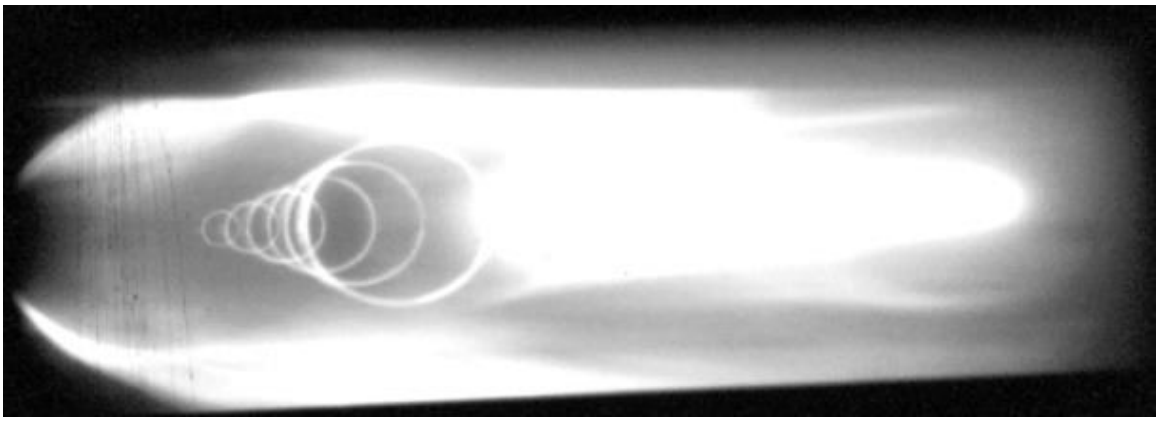

Figure 4-25 Streaks obtained by IMACON from experiment with wave shaper

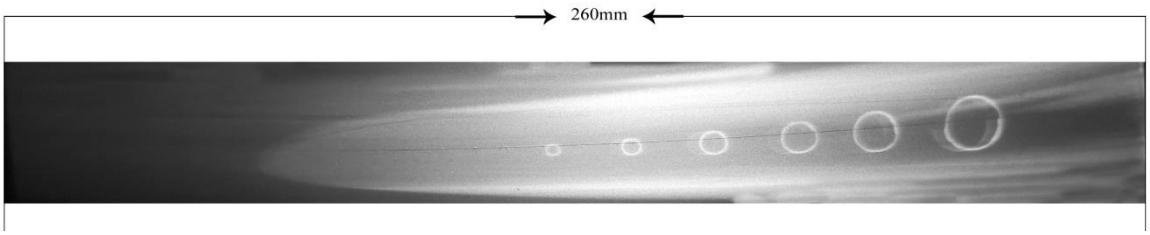


Figure 4-26 Streaks obtained by RMC from experiment with wave shaper

Data obtained from Figure 4-26 of the ring shaped streaks of experiment with wave shaper inside the high explosive is tabulated in Table 4-9 .Here the recording speed is adjusted to 9mm/μ sec. Groove distances under the heading “Dist. Travelled” in the table were already measured from the engineering drawing of perspex cone.

Table 4-9 Streak distances and shock velocities for experiment with wave shaper

| Experimental Times for Experiment With Wav Shaper | | | | | |
|---|---|---|---|---|---|
| Gauge Number | Streak Length | Time | Dist. Travelled | Shock Front Velocity | Error |
| 2-3 | $18^{+0.5}_{-0.0}$ | $2.000^{+0.056}_{-0.000}$ | 16.69 | 8345 | -226 |
| 3-4 | $18^{+0.0}_{-0.5}$ | $2.000^{+0.000}_{-0.056}$ | 17.04 | 8520 | 243 |
| 4-5 | $19^{+0.5}_{-0.0}$ | $2.111^{+0.056}_{-0.000}$ | 17.50 | 8289 | -213 |
| 5-6 | $16^{+0.5}_{-0.0}$ | $1.778^{+0.056}_{-0.000}$ | 15.86 | 8921 | -270 |
| 6-7 | $21^{+0.5}_{-0.0}$ | $2.333^{+0.000}_{-0.056}$ | 21.22 | 9094 | -211 |

Experimentally calculated shock front velocities from the circular streaks on the surface of the liner is plotted below in Figure 4-28

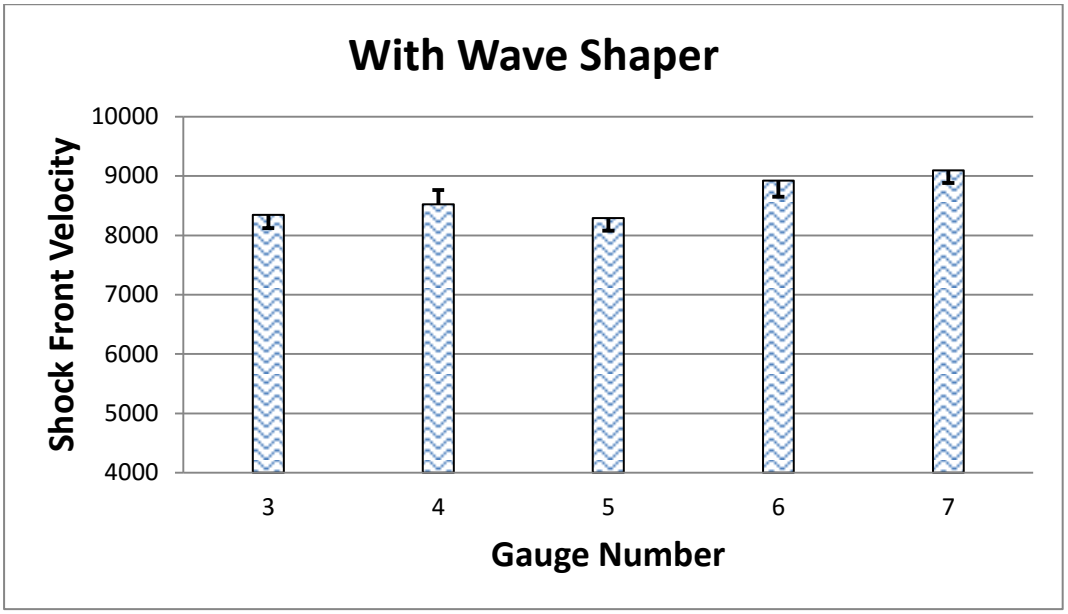


Figure 4-27 Experimental shock front velocities with wave shaper

Time of arrival of the wave front at the specified locations of grooves is found by placing fixed gauges. These arrival times and their corresponding velocities are tabulated in Table 4-10 .

Table 4-10 Shock arrival time and velocity for experiment with wave shaper

| Gauge Number | Shock Arrival Time | ***Simulation Data*** | | |
|---|---|---|---|---|
| 2 | 13.45 | Time Diff. (μ s) | Cone Dist.(mm) | Shock Velocity (m/s) |
| 3 | 15.060 | 1.61 | 16.69 | 10366 |
| 4 | 16.780 | 1.72 | 17.04 | 9907 |
| 5 | 18.590 | 1.81 | 17.50 | 9669 |
| 6 | 20.240 | 1.65 | 15.86 | 9612 |
| 7 | 22.350 | 2.11 | 21.22 | 10057 |

Shock front velocities calculated by simulation from gauge times on the surface of liner having wave shaper are plotted in Figure 4-28.

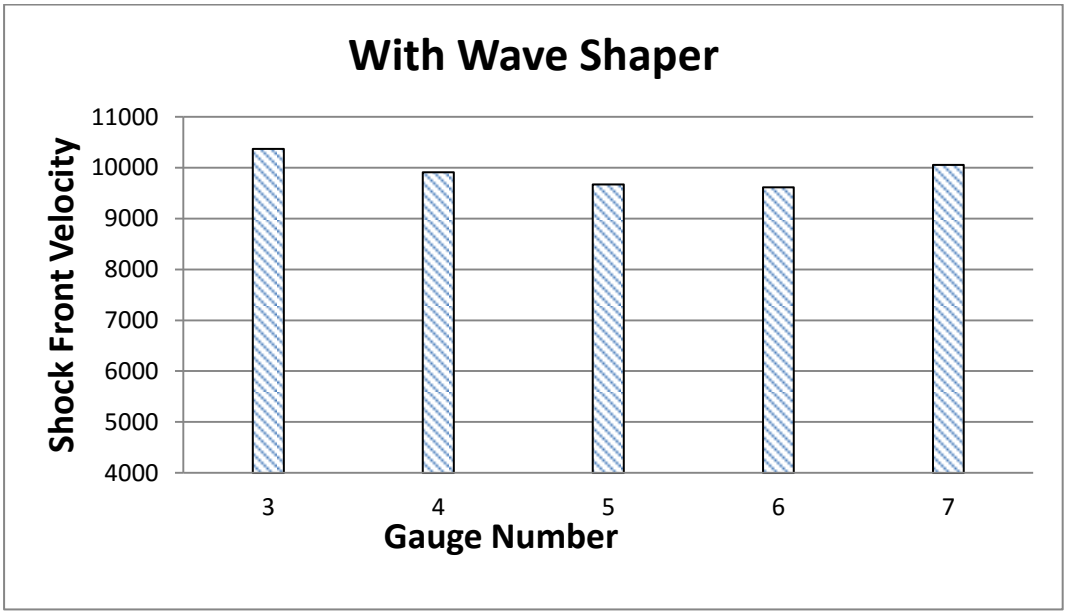


Figure 4-28 Simulation shock front velocities from with Wave Shaper

A comparison of both the experimental and simulation shock front velocities is given in Figure 4-29 . At gauge number three there is very drastic change from the

normal. This is because of the corner turning of the wave front and the wave front arrives at gauges number 2 and 3 with a time difference of only 2 µsec. This effect is due to the wave shaper which invokes the top attack of the shock front to get maximum penetration and low perturbations. Thus wave shaper made of perspex is performing its duty of wave shaping very well.

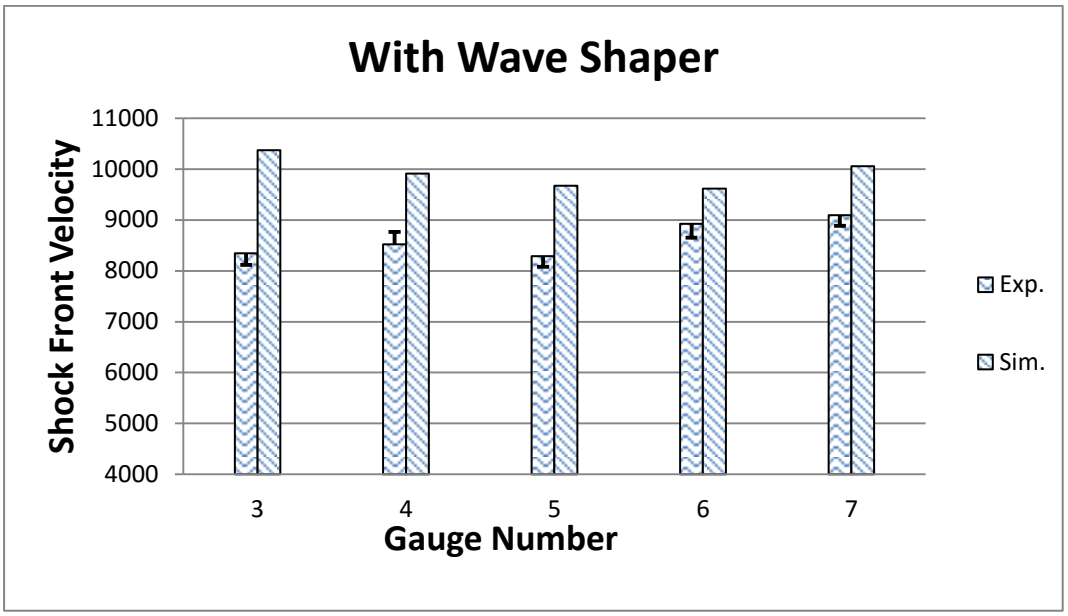


Figure 4-29 Comparison of experimental and simulation velocities

# Discussion and Conclusion

## *5.1 Discussion*

Figure 4-12shows that circular grooves made on the perspex cone appear somewhat oval in shape. These defects are due to viewing angle of the camera. This oval effect is best understood with the help of Figure 5-1. Here a circular object is photographed from two different viewing angles on the left it is perfectly circular while on the right side we can see that the same circular object now looks

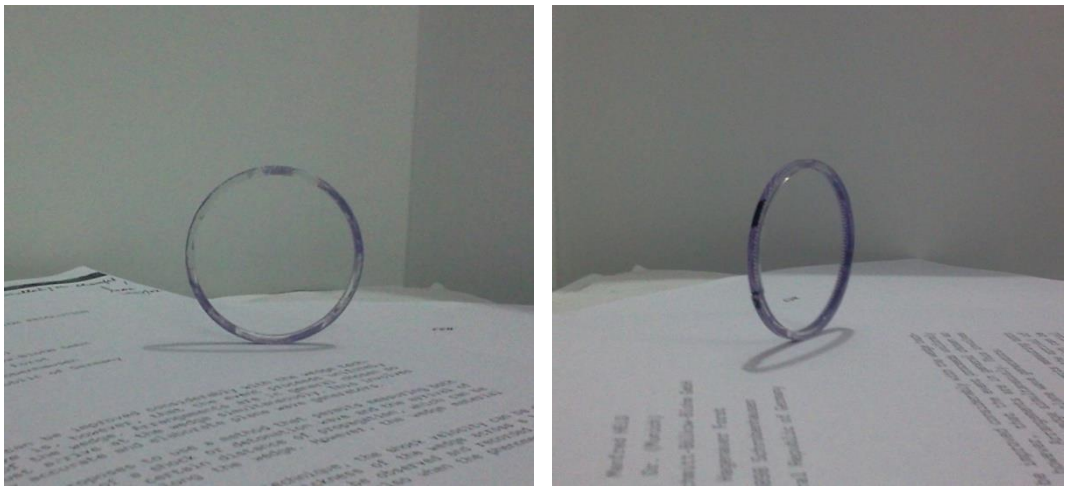

Figure 5-1 Photograph of the same object at different angles

oval which is observed in both the experiments.

Mirror for reflection into the camera must be parallel to the axis of the cone; that is it must be perpendicular to the face of the cone but in the experimental setup it was making an angle to the axis of the cone. Secondly the camera was also not perpendicular to the mirror which should be, for obtaining better results.

Average shock front velocities calculated from streaks given in Figure 4-21 and Figure 4-26 have lower values than simulation results. Reasons for the lower values of shock front velocities are

I. The experiment geometry is not suitable for shock front velocity. The charge geometry must be cylindrical of certain diameter and length [30] Shock front velocity depends on the diameter of the charge and as the diameter of charge increases its velocity increases too but this change in almost negligible when certain diameter is reached. When diameter of the charge is somehow less than critical diameter explosive will not detonate. This change in shock front velocity is because of the energy losses by the explosive to the surrounding medium.[31]

II. Simulation gives always ideal results while in experiment we have energy losses from the exterior boundary.

III. Experimental setup also contains some kind misalignments which may be minute but its effects are deteriorating on shock front velocity as well as jet penetration.

As symmetry of a shaped charge device is very important for the penetration performance since the whole process starting from the liner collapse is theoretically an axisymmetric phenomenon[32]. Figure 4-11 shows that the diameter of the dots is increasing with time and both the dots are equidistant from the central axis which shows that the detonation in first experiment without wave shaper is perfectly centred. This also gives that there is perfect alignment between the perspex cone and the high explosive; between high explosive and the casing. Streaks also shows that the detonation is perfectly symmetric and there is no off centre initiation.

Resultant streaks from experiment with wave shaper given in Figure 4-26 also shows that the diameter of streaks increases with time and space. This gives that there is complete centricity between the main charge, perspex mask and casing. It indicates that initiation is from the centre and propagation of shock is also uniform with reference to the charge axis.

Arrival time of shock front on the surface of the mask suggests that in the same fashion the shock front will arrive if the mask is replace by the liner. It was observed that the shock front velocities are higher near the apex and average shock

front velocity is varying along the surface of the mask. This is because the shock front strikes the gauge points near the apex from the top which results in higher values. This phenomenon is clear from the figures obtained by the simulation of the two set of experiments one with wave shaper and other without wave shaper.

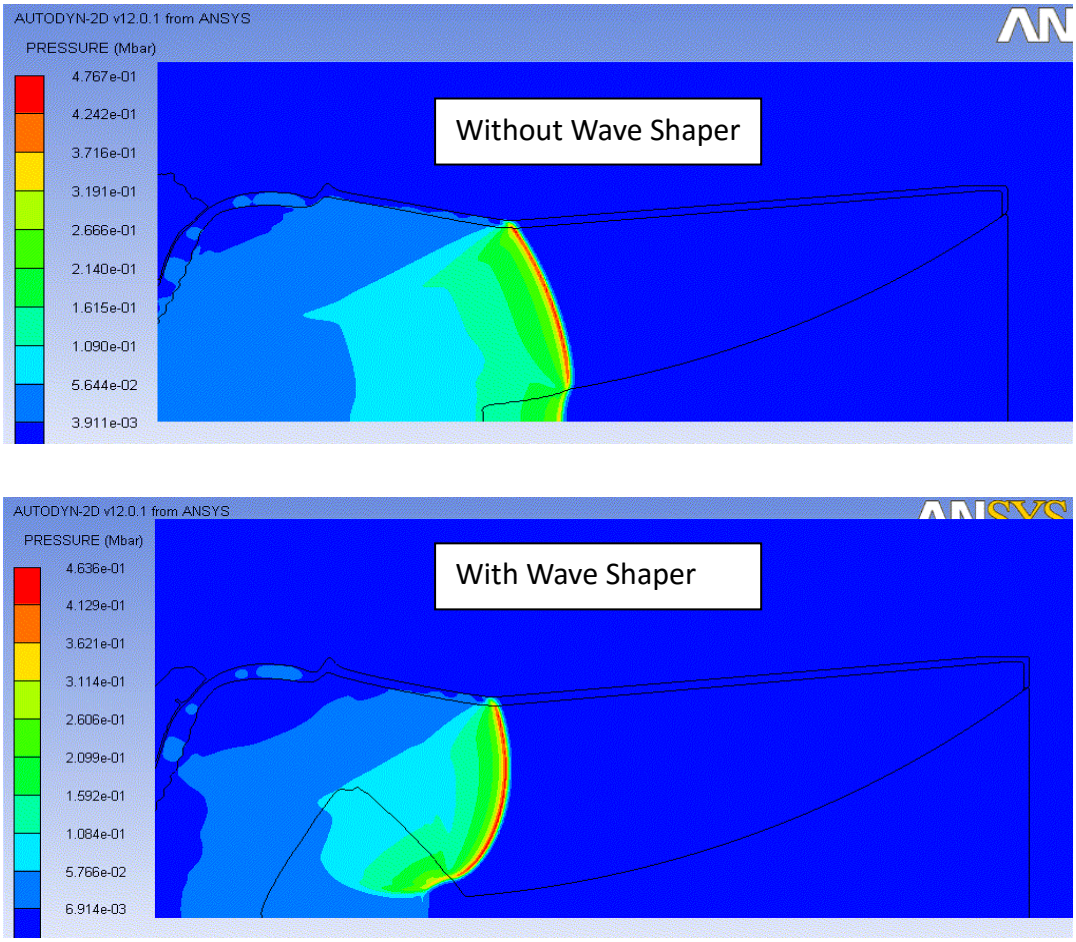


Figure 5-2 Wave front comparison at 11 µ sec.

In simulation without wave shaper it is observed that the wave front is spreading out in a circular pattern as expected from a normal detonation. While in simulation where perspex wave shaper is inserted the front can't spread out in circular fashion because of the perspex wave shaper which is inert and does not feed energy to the wave front but instead shock front is damped slowly in wave shaper. We can say that the shock front in the explosive is moving ahead of the front in the Perspex and the front strikes the mask from top also called top attack. This is the reason that we get higher values of shock front velocities in case of perspex especially in

the apex region of the mask immersed in the explosive as compared to that without wave shaper.

## 5.2 Conclusion

These experiments were successfully performed to observe the shock front arriving along the entire length of the perspex mask. In these experiments copper liner was replace by perspex mask. From experiment with wave shaper it is clear from the streak that shock front strikes the mask from the top near the apex, which was our objective. This top attack will allow more material of the liner to flow into the jet. The jet so produced is more uniform and there is less off axis perturbations. All these help to improve the penetration. Shock front velocities calculated from both the experiment does not match to that available in literature. The reason is that for velocity calculation we need a cylindrical shape explosive of the required diameter and length; and we must measure the arrival time of the shock in a straight line. If these conditions were not met we will get variations in velocities. Because of all these limitation the standard deviation among the velocities taken at specified location on the surface of the perspex mask in experiment without wave shaper is ±0.554.While the same data taken from the simulation gives a standard deviation of ±0.449. Similarly the standard deviation between the velocities taken at specified location on the surface of mask in experiment with wave shaper is ±0.489 and when the data from simulation was examined it gave a deviation of ±0.306. Standard deviations show that the data obtained in experiment with wave shaper has less variation as compared to experiment without wave shaper in both experimental and in simulation results. Results obtained from experiment with wave shaper are closer to the already established shock front velocity.

## 5.3 Recommendations

As shock front velocities measured from both the experiments do not match to that obtained from simulations. This effect can be minimized or in other words to get better timings from the experiment the grooves width on the perspex cone must be kept at minimum so as to get a sharp streak otherwise we will get blur streaks. In our case the width of grooves on the perspex cone was kept at 2±0.1mm .it was not possible to get a fine groove because of the unavailability of machining tool and

due to the low melting point of the perspex. Hence this experiment may be modified to address this disagreement or a relation may be established between the observed experimental timings and simulation timings. Another way to confirm appearance time of the streaks and shock front velocities is to use timing probes on the surface of the liner. These probes may be shortening probes which on shortening give a signal to multi-channel chronometer or these may be fibre optic probes which transmit the light to the acquisition system. It is to be noted that the fibre optic probes gives better results than its alternative shortening probes. The reason is that shortening probes efficiency does depends on its length and its resistance while in case of fibre optic only light is transmitted through the fibre which is independent of the fibre length. Light from the fibre optic cable is converted to electrical signal for further processing. This study does not include penetration comparison of two sets of experiment having wave shaper and without wave. To find the penetration comparison these two experimental setups having copper liner instead of Perspex mask should be fired against RHA.

# REFRENCES


1. Pugh, E.M., R. Eichelberger, and N. Rostoker, *Theory of jet formation by charges with lined conical cavities.* Journal of Applied Physics, 1952. **23**(5): p. 532-536.
2. *Article on the evolution of hand-held anti-tank technology*. Available from: Military.com.
3. Held, M., *Liners for shaped charges.* Journal of Battlefield Technology, 2001. **4**: p. 1-7.
4. Ugrcic, M. *The contribution to the optimization of detonation wave in the shaped charge construction*. in *19th International Symposium of Ballistics. Interlaken, Switzerland: International Ballistics Committee*. 2001.
5. Grove, B.M., J.F. Lands, and R.A. Parrott, *Shaped charges having reduced slug creation*. 2000, Google Patents.
6. Held, M., *Optical diagnostic of Shaped charge Jet.* 25 th international Congress on High Speed Photography and Photonics, 2003. **4948**(2003).
7. Cooper, P.W. and S.R. Kurowski, *Introduction to the Technoloy of Explosives*. 1996, United Stated of America: VCH Publishers. 204.
8. Molinari, J.F., *Finite element simulation of shaped charges.* Finite Elements in Analysis and Design, 2002. **38**(10): p. 921-936.
9. Junqing, H., et al., *The 3D Numerical Simulation of the Shaped Charge Jet Penetration through the Steel Target*, in *The 2nd International Conference on Computer Application and System Modeling (2012)*. 2012, Atlantis Press: China.
10. Katayama, M., et al., *Analysis of jet formation and penetration by conical shaped charge with the inhibitor.* International Journal of Impact Engineering, 1999. **23**(1): p. 443-454.
11. Eather, R.F. and N. Griffith, *Some Historical Aspects of the Development of Shaped Charges*. 1984, Royal Arlmament Research And Development Establishment: London. p. 25.
12. Evans, W.M. and A.R. Ubbelohde, *The Mechanism of Jet Formation*. 1941.
13. Hussain, G. and K. Sanaullah, *Comparative parametric numerical simulations of materials used as liners in the explosively formed projectiles (EFPs).* Nucleus, 2009. **46**(3): p. 301-309.
14. Held, M., *Shock profiles along a specimen.* Propellants Explosives Pyrotechnics, 1999. **24**(6): p. 360-365.
15. Taylor, G., *A formulation of Mr. Tuck's conception of Munroe jets.* The scientific papers of Sir Geoffrey Ingram Taylor, 1943. **3**: p. 358-362.
16. Birkhoff, G., et al., *Explosives with lined cavities.* Journal of Applied Physics, 1948. **19**(6): p. 563-582.
17. Hill, R., H. Mott, and D. Pack, *Penetration by Munroe Jets.* Armament Research Department, Report, 1944. **2**: p. 44.
18. Cowan, K. and B. Bourne. *ANALYTICAL CODE AND HYDROCODE MODELLING AND EXPERIMENTAL CHARACTERISATION OF SHAPED CHARGES CONTAINING CONICAL MOLYBDENUM LINERS.* in *19th International Ballistic Symposium*.

19. Held, M. *Streak technique in detonics*. in *17th Int'l Conference on High Speed Photography and Photonics*. 1987: International Society for Optics and Photonics.
20. Werneyer, K.D., C.J. Terblanche, and F. Majiet, *IMPROVED STREAK MASK DESIGN*, in *27TH INTERNATIONAL SYMPOSIUM ON BALLASTICS*. 2013: FREIBURG, GERMANY.
21. Held, M., *Verification of the equation for radial crater growth by shaped charge jet penetration.* International journal of impact engineering, 1995. **17**(1): p. 387-398.
22. Walter, W.P. and J.A. Zukas, *Fundamentals of Shaped Charges*, ed. S. Edition. 1998, USA: CMC Press, Baltimore, MD. 398.
23. Walters, W.P. and J.A. Zukas, *Fundamentals of shaped charges*. 1989: John Wiley.
24. Kok, R.W.O. and F.U. Deisenroth, *LIGHTWEIGHT PASSIVE ARMOUR FOR INFANTRY CARRIER VEHICLE.* 19th International Symposium of Ballistics, 2001: p. 961-967.
25. Held, M., *ERA Patents*. 2008: Germany.
26. Fluent, A., *12.0 User's Guide.* Ansys Inc, 2009.
27. AUTODYN, A., *Interactive Non-Linear Dynamic Analysis Software, Version 12, User's Manual.* SAS IP Inc, 2009.
28. Baker, E.L., *Modeling and optimization of shaped charge liner collapse and jet formation*. 1993, DTIC Document.
29. K.K., H.P. (2008) *GUIDE TO STREAK CAMERAS.*
30. Held, M., *Simultaneously gained streak and framing records offer a great advantage in the field of detonics.* Propellants Explosives Pyrotechnics, 2001. **26**(3): p. 148-155.
31. Cooper, P.W., *Explosives engineering*. 1996, USA: Wiley Vch Pub. 460.
32. Ayisit, O., *The influence of asymmetries in shaped charge performance.* International Journal of Impact Engineering, 2008. **35**(12): p. 1399-1404.